Detecting the Optic Disc Boundary in Digital Fundus Images Using Morphological, Edge Detection, and Feature Extraction Techniques

Arturo Aquino*, Manuel Emilio Gegúndez-Arias, and Diego Marín

***Abstract*—Optic disc (OD) detection is an important step in developing systems for automated diagnosis of various serious ophthalmic pathologies. This paper presents a new template-based methodology for segmenting the OD from digital retinal images. This methodology uses morphological and edge detection techniques followed by the Circular Hough Transform to obtain a circular OD boundary approximation. It requires a pixel located within the OD as initial information. For this purpose, a location methodology based on a voting-type algorithm is also proposed. The algorithms were evaluated on the 1200 images of the publicly available MESSIDOR database. The location procedure succeeded in 99% of cases, taking an average computational time of 1.67 s. with a standard deviation of 0.14 s. On the other hand, the segmentation algorithm rendered an average common area overlapping between automated segmentations and true OD regions of 86%. The average computational time was 5.69 s with a standard deviation of 0.54 s. Moreover, a discussion on advantages and disadvantages of the models more generally used for OD segmentation is also presented in this paper.**

***Index Terms*—Diabetic retinopathy, glaucoma, optic disc (OD) segmentation, retinal imaging, telemedicine.**

I. Introduction

DIABETIC retinopathy (DR) is a chronic disease which nowadays constitutes the primary cause of blindness in people of working age in the developed world [1]–[3]. The benefits that a system for automaticly detect early signs of this disease would provide have been widely studied and assessed positively by experts [4], [5]. In this sense, the OD plays an important role in developing automated diagnosis expert systems for DR as its segmentation is a key preprocessing component in many algorithms designed to identify other fundus features. The relatively constant distance between the OD and the fovea, can be used to help estimate the location of the latter [6]. On the other hand, to segment the vascular tree, vessel tracking methods need an initial seed vessel point. For this, pixels of vessels within the OD or in its vicinity have been used [7], [8]. In addition, OD segmentation can be useful in diagnosing automatically some diseases caused by DR. Finding the OD can be used to decrease false positives in the detection of regions of retinal exudates [9]. These injuries are a diagnostic key to grading the risk of macular edema.

OD segmentation is also relevant for automated diagnosis of other ophthalmic pathologies. One of them and maybe the most noteworthy is Glaucoma. It is the second most common cause of blindness worldwide [10]. Glaucoma is identified by recognizing the changes in shape, color, or depth that it produces in the OD [11]. Thus, its segmentation and analysis can be used to detect evidence of Glaucoma automatically.

The OD can be distinguished in eye fundus images as a slightly elliptical shape. Its size may vary significantly and different estimations have been made. Whereas Sinthanayothin *et al.* [6] stated that it occupies about one-seventh of the entire image, alternatively other authors have pointed out that OD size varies from one person to another, occupying about one-tenth to one-fifth of the image [7]. In color fundus images, the OD usually appears as a bright yellowish region, although this feature may also experience significant variations (Fig. 1).

OD segmentation is not an easy matter. Besides the variations in OD shape, size, and color pointed out previously, there are some additional complications to take into account. Contrast all around the OD boundary is usually not constant or high enough piecewise due to outgoing vessels that partially obscures portions of the rim producing "shadows." Another distractor is produced when peripapillary atrophy is present, as this produces bright areas just outside the OD rim which distort its shape. On the other hand, eye movement at the moment of retinography capture may also lead to slightly blurred images, making their automated analysis even more difficult. This problem can be avoided by simply discarding these images and retaking new ones. However, this method is not usually applied as their quality is usually good enough for human visual inspection.

This paper presents a new template-based method for OD segmentation. Firstly, an OD-containing sub-image is extracted: an OD pixel and its surrounding region (a surrounding region wide enough to include the whole OD) are selected. With this purpose, an OD location methodology is also proposed here. Then,

Manuscript received April 05, 2010; revised May 25, 2010; accepted June 05, 2010. This work is part of the Expert System for Early Automated Detection of DR by Analysis of Digital Retinal Images Project, supported and funded by the Health Ministry of the Andalusian Regional Government (Spain). *Asterisk indicates corresponding author.*

*A. Aquino is with the Department of Electronic, Computer Science and Automatic Engineering, "La Rábida" Polytechnic School, University of Huelva, 21071 Huelva, Spain (e-mail: arturo.aquino@diesia.uhu.es).

D. Marín is with the Department of Electronic, Computer Science and Automatic Engineering, "La Rábida" Polytechnic School, University of Huelva, 21071 Huelva, Spain (e-mail: diego.marin@diesia.uhu.es).

M. E. Gegúndez-Arias is with the Department of Mathematics, "La Rábida" Polytechnic School, University of Huelva, 21071 Huelva, Spain (e-mail: gegundez@uhu.es).

Color versions of one or more of the figures in this paper are available online at http://ieeexplore.ieee.org.

Digital Object Identifier 10.1109/TMI.2010.2053042

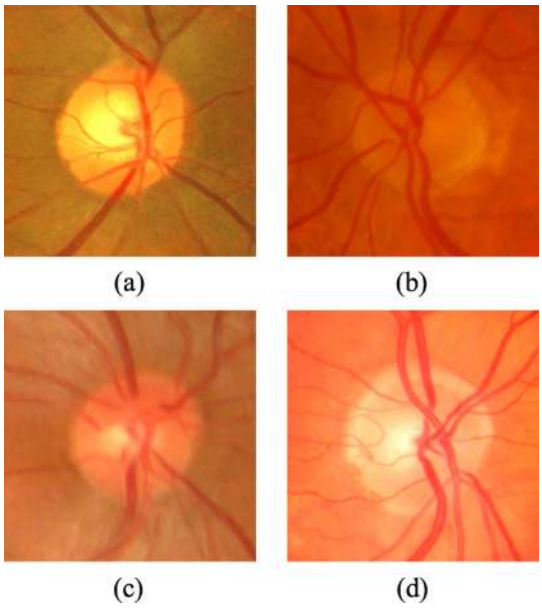

Fig. 1. Examples of OD appearance. (a) Yellowish OD. (b) Brownish OD. (c) Reddish OD. (d) Whitish OD.

the OD boundary is extracted in parallel from both the red and green channels of this sub-image by means of morphological and edge detection techniques. Both OD boundaries are approximated by a circumference using the Circular Hough Transform. The "better" of these results is finally selected. This paper also includes a study on advantages and disadvantages involved by the use of circular, elliptical and deformable models for OD segmentation. The results of this study strengthen the hypothesis of the suitability of circular models for this purpose and show evidence that the circular approach offers good compromise between success rate, quality, and efficiency.

II. Overview of State of Art

The available works related to OD processing in eye fundus color images can be grouped into two distinct categories: *location* and *segmentation* methods. The former works focus on finding an OD pixel (generally representative of its center). On the other hand, the latter works estimate the OD boundary. Within this category, a general distinction can be made between *template-based* methods (methods for obtaining OD boundary approximations) and methods based on *deformable models* or *snakes* for extracting the OD boundary as exactly as possible. With regard to location methods, Synthanayothin *et al.* presented a method [6], [12] where the images were preprocessed by applying an adaptative local contrast enhancement to the intensity channel of the HSI color space. The OD center location was identified using the variance of intensity produced by the blood vessels within the OD. Hoover and Goldbaum [13], [14] located the center of the OD using the vasculature origin. They determined where all the vessels converged by means of a voting-type algorithm called fuzzy convergence. Another method that uses the convergence of the vessels to detect the OD center was proposed by Foracchia *et al.* [15]. The four main vessels originating from the OD were geometrically modeled using two parabolas, and the OD position was located as their common vertex. Inspired by previous works, Youssif *et al.* [16] presented an OD location method based on a vessels' direction matched filter. As a first step a binary mask was generated followed by image brightness and contrast equalization. Finally, the retinal vasculature was segmented, and the directions of the vessels were matched to the proposed filter representing the expected vessels' directions in the vicinity of the OD.

With regard to segmentation methods and concretely to works based on deformable models, Osareh *et al.* [17] located the OD center by means of template matching and extracted its boundary using a snake initialized on a morphologically enhanced region of the OD. Lowell *et al.* [18] also localized the OD by means of template matching as well as also selected a deformable contour model for its segmentation. Specifically, they used a global elliptical model and a local deformable model with variable edge-strength dependent stiffness. Another deformable model-based approach was presented in [19]. The snake behavior against vessel occlusion was improved and the model was extended in two aspects: knowledge-based clustering and smoothing update. Thus, the snake deformed to the location with minimum energy and then self-clustered into two groups, which were finally updated by the combination of both local and global information. Regarding template-based methods, Wong *et al.* [20] proposed: 1) OD location by means of histogram analysis and initial contour definition according to the previously obtained location, and 2) a modified version of the conventional level-set method was subsequently used for OD boundary extraction from the red channel. This contour was finally fitted by an ellipse. Another template-matching approach for OD segmentation is the Hausdorff-based template matching presented by Lalonde *et al.* [21]. Initially, they determined a set of OD candidate regions by means of multiresolution processing through pyramidal decomposition. For each OD region candidate, they calculated a simple confidence value representing the ratio between the mean intensity inside the candidate region and inside its neighborhood. The Canny edge detector and a Rayleigh-based threshold were then applied to the green-band image regions corresponding to the candidate regions, constructing a binary edge map. As final step, using the Hausdorff distance between the edge map regions and circular templates with different radii, they decided the OD among all the candidates. On the other hand, although they do not belong to the two reviewed categories, works [22]–[24] proposed other relevant OD segmentation methods. Walter and Klein [22] found the OD contour through the watershed transformation. For OD detection, its center was previously approximated as the centroid of the largest and brightest connected object in a binary image obtained by thresholding the intensity channel. Reza *et al.* [23] also used the watershed transformation for OD segmentation. Firstly, the green channel was preprocessed for image condition enhancement. Then, morphological opening, extended maxima operator and minima imposition were finally used to apply the watershed transformation for bright structure segmentation. Finally, although applied to stereo images, it is worth mentioning the novel OD segmentation approach presented by Abràmoff *et al.* [24]. Pixel feature classification by means of a k-nearest neighbor classifier was used in this case for OD segmentation in stereo color photographs.

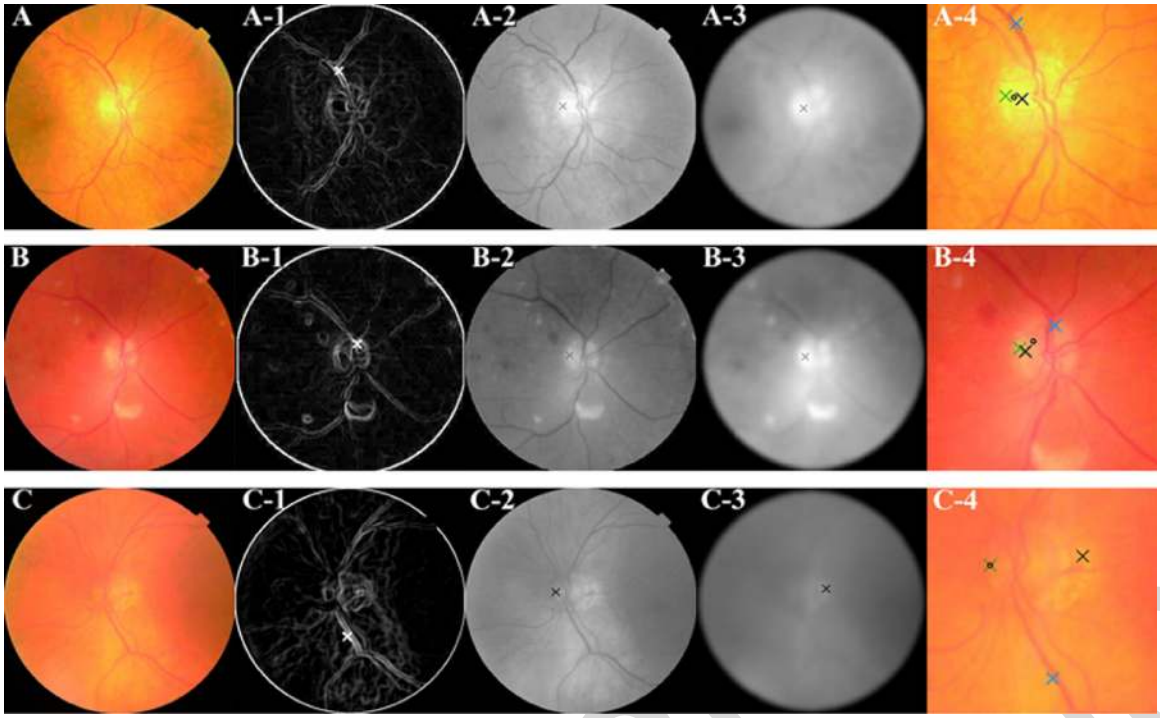

Fig. 2. ODP determination: (A), (B), and (C) Original images. (A-1), (B-1), and (C-1) OD pixels rendered by the maximum difference method. (A-2), (B-2), and (C-2) OD pixels rendered by the maximum variance method. (A-3), (B-3), and (C-3) OD pixels rendered by the low-pass filter method. (A-4), (B-4), and (C-4) Final ODP determination (black circumference): in (A-4), although the OD pixel of the maximum difference method is not properly selected, the ODP is successfully located; in (B-4) the ODP selected is the centroid of the three OD pixels; in (C-4), since the three OD pixels are far from their centroid, the ODP selected is the OD pixel from the maximum variance method.

III. Methodology

The aim of this work is to introduce a new methodology for OD segmentation that obtains a circular boundary approximation. It needs as initial information the coordinates of a pixel located within the OD. To this effect, in order to complement the presented segmentation methodology, a simple but reliable and very fast OD location methodology is also proposed to obtain the required OD pixel. It must be stressed that any other location method could be used for this purpose.

All values of parameters, constants and window sizes given in this section refer to retinas of 1046 pixels in diameter. For different image resolutions, all of these values would have to be scaled.

A. Optic Disc Location

The location methodology obtains a pixel [called Optic Disc Pixel (ODP)] that belongs to the OD. It comprises three independent detection methods. Each method obtains its own OD candidate pixel. The final ODP is selected by taking into account the three previous candidate pixels and their location with respect to their average point (centroid). For this, a voting procedure comprising the following cases is applied.

- If the three OD candidate pixels are close to the centroid (closer than one-fifth of the image, maximum OD diameter estimation [7]): the selected ODP is the centroid.
- If only two candidates are close to the centroid: the selected ODP is the average point in these two referred pixels.
- Otherwise, the selected ODP is the candidate pixel obtained with the most reliable method (performed tests show this is the maximum variance method described below).

The three developed methods work on the green channel of the RGB color space as this is the one that provides the best contrast [25]. This gray scale image will be denoted as I. A description of these methods, illustrated in Fig. 2 by three examples of their application to different eye fundus images, is presented as follows.

- Maximum Difference Method: The OD usually appears as a bright region in eye fundus images. Moreover, the vascular tree formed by the "dark" blood vessels emerges in the disc. This is why the maximum variation of the gray levels usually occurs within the OD. This maximum is used by this method to select its OD pixel.
  A median filter of 21×21 is applied beforehand to I in order to remove nonsignificant peaks in the image. If I_M denotes this filtered image, the OD pixel from this method is decided according to the following equation:
$$P_{\mathrm{MDM}} = \arg\limits_{(i,j)} \left(\max \left\{ (I_M)_W^{\mathrm{MAX}}(i,j) - (I_M)_W^{\mathrm{MIN}}(i,j) \right\} \right) \quad (1)$$
  where $(I_M)_W^{\mathrm{MAX}}$ and $(I_M)_W^{\mathrm{MIN}}$ are, respectively, the maximum and the minimum values of the pixels in I_M within a window W of size 21×21 centered on a pixel (i,j) (see examples in Fig. 2, images A-1, B-1, and C-1).
- Maximum Variance Method: This method is based on the same properties as the previous one. It calculates the statistical variance for every pixel by using a 71×71 centered

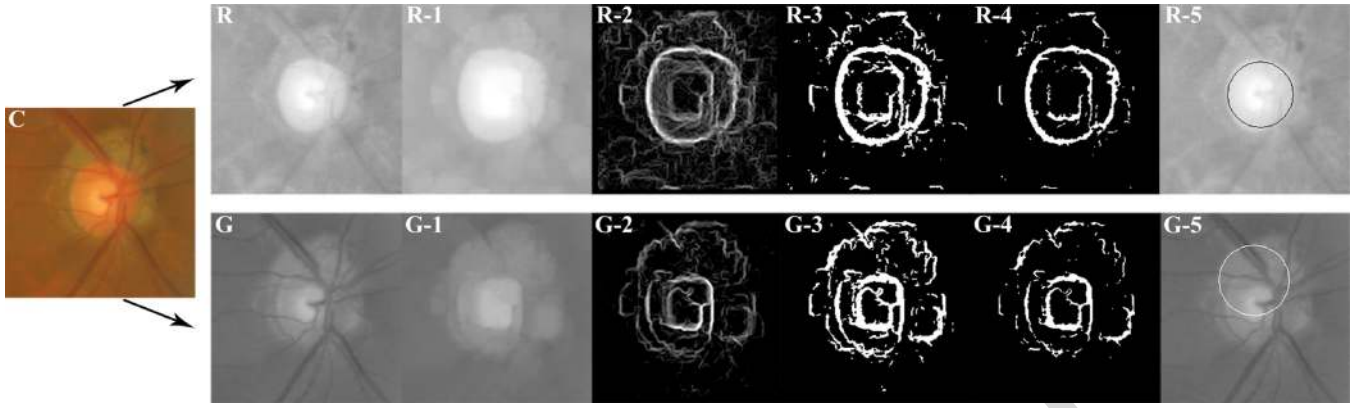

Fig. 3. Illustration of the process for the calculation of the circular OD boundary approximation: (C) Initial RBG sub-image containing an OD affected by peripapillary atrophy. On the right, the top row shows the process performed on the red channel, whereas the bottom corresponds to the process applied to the green component. (R) and (G) Subimages extracted from the red and green channels of (C), respectively. (R-1) and (G-1) Vessel elimination. (R-2) and (G-2) Gradient magnitude image. (R-3) and (G-3) Binary image. (R-4) and (G-4) Cleaner version of the binary image. (R-5) and (G-5) Circular OD boundary approximation. The scores obtained in the Circular Hough Transform algorithm are, 264 for segmentation in (R-5) and 130 for segmentation in (G-5), so the segmentation selected would be the one performed on the red channel.

window. On the other hand, a set of "bright" pixels is obtained by automatic blue-channel thresholding according to the Otsu method [26]. The OD pixel returned by this method is the maximum variance pixel showing at least 10 "bright" pixels in its neighborhood (established by means of a 101×101 pixel window) (see Fig. 2, images A-2, B-2, and C-2). The window sizes selected to compute the variance and to establish the neighborhood criteria, were set with the aim of obtaining the best location performance on a set of 1200 fundus images (this database is described in Section IV).

- Low-Pass Filter Method: The OD pixel of this method is the maximum gray-level pixel in a low-pass filtered image. Although the OD is usually the brightest area in a retinography, the pixel with the highest gray level could not be located within it. In many cases, this pixel may be inside other small bright regions. In order to smooth out these distractors, the image I is transformed to the frequency domain and filtered by the Gaussian low-pass filter defined as follows:

$$H(u,v) = \exp\left(\frac{-D^2(u,v)}{2D_0^2}\right) \tag{2}$$

where $D(u,v)$ is the Euclidean distance between the point (u,v) and the origin of the frequency plane, and D_0 is the cutoff frequency with a value of 25 Hz. The highest gray-level pixel in the filtered image returned to the spatial domain is the result of this method (Fig. 2, images A-3, B-3, and C-3).

The result of the final ODP selection process is illustrated by the three examples of application of the methodology shown in Fig. 2. In the first example (Fig. 2, images A to A-4), it can be confirmed that although the pixel returned by the maximum difference method is outside the disc, it is discarded and the ODP is successfully selected. In the second example (Fig. 2, images B to B-4), pixels returned by the three methods are close, so the location of the ODP is the location of their centroid. In the last example (Fig. 2, images C to C-4), the three partial results are far from their centroid, so the final ODP is the OD pixel found by the maximum variance method.

B. Optic Disc Boundary Segmentation

The method proposed in this paper is performed on an RGB sub-image of the original retinography. By this way, robustness and efficiency in OD segmentation are increased as it reduces the search space and decreases the number of artifacts and distractors present in the whole image. So, as a first step, a 400×400 RGB sub-image is extracted centered on an OD pixel provided by the OD location methodology previously presented, or by any other if desired.

Although the green component of an RGB retinography is the one with highest contrast [25], the OD is often present in the red field as a well-defined white shape, brighter than the surrounding area. When contrast between the OD shape and its environment in this color field is high enough, the OD can usually be segmented better than in the green field. At other times, the OD is not discernable in the red component and has to be segmented in the green one. To exploit this feature, the OD segmentation is performed in parallel on the two components and the "better" of the two segmentations is ultimately selected. The proposed procedure firstly employs an special morphological processing to eliminate blood vessels. Then, a binary mask of the OD boundary candidates is obtained by applying edge detection and morphological techniques. Finally, the Circular Hough Transform is used to calculate the circular approximation of the OD.

1) Elimination of Blood Vessels: Consider the gray-level image I from the red or green field of the sub-image containing the OD (Fig. 3, images R and G). As was discussed, blood vessels within the OD act as strong distractors, so they should be erased from the image beforehand. The vasculature is piecewise linear and can be considered as a structure composed of many such connected linear shapes with a minimum length L and a maximum width W, where usually $W \ll L$ (see Heneghan *et al.* [27]). These linear shapes are formed, as a general rule, by a set of pixels with an almost constant gray-level value, with

this value being somewhat lower than the gray-level values of non-vessel pixels in their vicinity. Using a rotating linear structuring element B of width 1 and length $L_1 \gg W$, a linear shape can be detected by calculating the statistical variance of gray-level values of pixels along it. The rotation associated with the minimum value will be that in which the vessel contains B and, conversely, the rotation with the highest value will refer to the situation in which B crosses the linear shape. Thus, vessels can be removed from image I by finding, for every pixel, the rotation which produces the maximum gray level variance value and taking the maximum gray-level in the neighborhood defined by the structuring element at that rotation (see effects at Fig. 3, images R-1 and G-1). Mathematically this can be expressed as

$$I_{\neg V}(i,j) = I_{B_r}^{\mathrm{MAX}}(i,j) \tag{3}$$

where

$$r = \arg_k \left(\max \left\{ I_{B_k}^{\mathrm{VAR}}(i,j),\ k = 1, \ldots, 12 \right\} \right) \tag{4}$$

B_r represents structuring element B at rotation r determined by (4). Twelve rotations of the structuring element each 15° apart were used. The length L_1 of the structuring element should be chosen so as to cross vessels in order to erase them by applying (3). Taking into account the study proposed by Heneghan *et al.* in [27], the value for this parameter was set to 27. This operation produces an OD enlargement of L_1 pixels in all directions. This will be considered at the end of the processing.

2) Obtaining Od Boundary Candidates: The OD boundary represents the frontier between the OD and the background. It is characterized by a sudden variation in gray levels, with these values higher within the OD than in its surroundings. So, the OD boundary can be detected by measuring the gradient magnitude of gray-level changes in small neighborhoods of the image. Firstly, a mean filter is applied to eliminate pixel values unrepresentative of their environment. Then, the Prewitt edge detector [28] is used to obtain a gradient magnitude image (hereafter I_{GM}). This operator estimates image edge and orientation by convolving two 3×3 kernels which approximate derivatives for horizontal and vertical changes. The gradient magnitude image is finally obtained by taking the module of partial derivative values for every pixel. Thus, I_{GM} is an image which contains information on edges, specifically on the location and intensity of local gray-level variations (Fig. 3, images R-2 and G-2). As the blood vessels were previously erased, in general the most significant edges in the gradient image correspond to the OD boundary. Thus, a binary mask of OD boundary candidates can be produced by thresholding the image I_{GM}.

As stated before, there is great variability in OD appearance, and the contrast level between the OD and the background may vary quite substantially. That is why it is not suitable to establish a unique threshold for any image. The Otsu thresholding method [26] automatically decides a threshold for a gray-level image by assuming that it is composed of two sets, the background and the foreground. Then, the method establishes the optimum threshold T_{OTSU} by maximizing the between-class variance. Using this threshold, a first binary mask of OD boundary candidates is given by a simple binarization operation (see Fig. 3, images R-3 and G-3)

$$I_B(i,j) = \begin{cases} 0, & \text{if } I_{\mathrm{GM}}(i,j) \leq T_{\mathrm{OTSU}} \\ 255, & \text{if } I_{\mathrm{GM}}(i,j) > T_{\mathrm{OTSU}}. \end{cases} \tag{5}$$

This image can contain some noise caused by small rims present in the original image and detected in I_{GM}. So, the definitive binary mask of OD boundary candidates is obtained by cleaning I_B by means of morphological erosion (Fig. 3, images R-4 and G-4),

$$I_{\mathrm{BM}}(i,j) = (I_B)_C^{\mathrm{MIN}}(i,j) \tag{6}$$

where C is a circular structuring element with a diameter of five pixels. This operation reduces the OD radius in two pixels.

3) Final OD Boundary Segmentation: The Hough Transform [29] is widely used in Computer Vision and Pattern Recognition for detecting geometrical shapes that can be defined by parametric equations. Based on the primitive Hough Transform [29], the Circular Hough Transform was outlined by Duda *et al.* [30] and later improved and extended by Kimme *et al.* [31]. It aims to find circular patterns within an image. It is used to transform a set of feature points in the image space into a set of accumulated votes in a parameter space. Then, for each feature point, votes are accumulated in an accumulator array for all parameter combinations. The array elements that contain the highest number of votes indicate the presence of the shape. A circumference pattern is described by the parametric equation of the circumference, defined as

$$(x-a)^2 + (y-b)^2 = r^2 \tag{7}$$

where (a,b) are the coordinates of the circle center and r is the radius. So, the circular shapes present in I_{BM} can be obtained by performing the Circular Hough Transform on this image. It can be defined as

$$(P_c, r) = \mathrm{CHT}(I_{\mathrm{BM}}, r_{\min}, r_{\max}) \tag{8}$$

where $P_c = (i_c, j_c)$ and r are respectively the center position and the radius that define the circular shape with the highest punctuation in the Circular Hough Transform implemented by CHT. The radius r is restricted to be between $r_{\min}$ and $r_{\max}$, values which are one-tenth and one-fifth of the image [7] divided by two (as these measurements refer to OD diameter estimation). The minimum radius restriction reduces the probability of considering the OD cup, while the maximum radius restriction eliminates candidates with too wide areas. The obtained r value must be corrected due to the effects of (3) and (6). The vessel elimination performed in (3) enlarged the OD 27 pixels and the erosion operation in (6) produced a two-pixel reduction, so the r value has to be reduced by 25.

As previously commented, this processing is applied in parallel to the green and red channels. Thus, two OD approximations are obtained. The one with the higher score in the Circular Hough Transform algorithm is then selected as the definitive circular OD boundary approximation (Fig. 3, images R-5

TABLE I
RESULTS OF THE CIRCULAR HOUGH IN TERMS OF PERCENTAGE OF IMAGES PER OVERLAPPING INTERVAL AND AVERAGE OVERLAPPING OF THE WHOLE SET

	$S \geq 0.95$	$S \geq 0.90$	$S \geq 0.85$	$S \geq 0.80$	$S \geq 0.75$	$S \geq 0.70$	$\overline{S}$
"CircularGoldStandard"	27%	87%	96%	99%	99%	100%	0.92
CircularHough (this work)	**7%**	**46%**	**73%**	**84%**	**90%**	**93%**	**0.86**
Hausdorff-BasedTemplateMatching [21]*	2%	25%	45%	70%	77%	85%	0.81
CircularHough / "CircularGoldStandard"	**26%**	**53%**	**76%**	**85%**	**91%**	**93%**	**0.93**

* This results were obtained on a local database composed by 40 images.

and G-5). This score quantifies the point by point matching degree between the estimated circumference and the fitted shape in I_{BM}. Therefore, higher scores generally involve better OD border extraction and, hence, better segmentation quality. Moreover, the selection of the correct candidate is also favored by the fact that the score of this algorithm is an absolute and not a relative measure. This implies that the selected maximum-score criterion tends to select longer candidate circumferences. This is especially useful when the OD cup is wide enough to be considered a candidate, as it leads to an increased probability of selecting the correct candidate between the cup and the true OD boundary.

IV. TESTING AND RESULTS

We used in this study the publicly available MESSIDOR database [32], kindly provided by the Messidor program partners. It contains 1200 eye fundus color images of the posterior pole acquired by the Hôpital Lariboisière Paris, the Faculté de Médecine St. Etienne and the LaTIM–CHU de Brest (France). 800 of these images were captured with pupil dilation (one drop of Tropicamide at 10%) and 400 without dilation, using a Topcon TRC NW6 non-mydriatic retinograph with a 45° FOV. The images are 1440×960, 2240×1488, or 2304×1536 pixels in size and 8 bits per color plane and are provided in TIFF format. 540 images are from patients not affected by DR and 660 correspond to patients affected by the illness. To prevent the inclusion of any kind of skew, although some images are not suitable for processing (i.e., images too blurred or with severe enough cataract), no exclusion criteria was applied. To make evaluation of the algorithm performance on this database possible, the OD rim was manually delimited by experts producing by this way a gold standard set.

Although database images are provided in TIFF format, they were JPEG compressed at a ratio of 1:35 for testing. It was done for assessing algorithm performance under conditions established in the protocols defined by the organism that funded these investigations, the Andalusian Health Service, relating to image file size. This restriction is imposed as, using this kind of compressed format, storage requirements as well as latency in exchanging images via the internet are drastically reduced. Moreover, we performed tests on image resolution for the location and the segmentation methodologies, scaling down the images. These tests revealed that the results provided by both methods are independent and stable in spite of decreasing image resolution down to 300×300 for OD location and 640×640 for OD segmentation. Therefore, the methodologies presented are actually applied to images of these sizes. Any image of any resolution is reduced to 300×300 and 640×640 for OD location and OD segmentation respectively and the processes are performed scaling the window sizes and parameters to these resolutions. So, the results in this section were obtained applying these reductions.

Algorithm performance was evaluated by measuring the overlapping degree between the true OD regions in "gold standard" images and the approximated regions obtained with the described approach. The proposal by Lalonde *et al.* [21] was used with this purpose: an overlapping score S is defined to measure the common area between a true OD region T and a detected region D as

$$S = \frac{\mathrm{Area}\,(T \cap D)}{\mathrm{Area}\,(T \cup D)}. \tag{9}$$

Since the proposed algorithm segments the OD by approximating its shape by a circumference, for a better evaluation of its behavior, it is also interesting to get to know how far its results are from the maximum results reachable with this template-based approach. With this purpose, a "circular gold standard" set was created by calculating the best circular approximations for all true OD contours in the "gold standard" set by using (8). Then, the common area between the regions in the "gold standard" and these best circular approximations in the "circular gold standard" were calculated also according to (9). Therefore, the average of these values may be considered the upper limit of average common overlapping for an automatic OD segmentation using a circular approximation. So, generalizing, this experiment, apart from being interesting for better algorithm evaluation, provides an interesting objective measurement of the maximum OD area which can be covered by a circle. Therefore, it is an appropriate measure to assess the general suitability of OD segmentation using a circular approximation.

The algorithm presented in this paper (*CircularHough*) was applied to calculate the overlapping S defined in (9) for the 1200 images in the MESSIDOR database. This metric was also computed using the "circular gold standard" set (*CircularGoldStandard*). The results for both methods are summarized in Table I[1]. This table shows the percentage of images for different intervals of S values, as well as average overlapping $\overline{S}$ for the whole set of images. These overlapping measures corresponding to the *CircularHough* algorithm normalized by the results of the *CircularGoldStandard* are also shown in the last row. As shown in this table, overlapping between the hand-labelled OD region and *CircularHough* algorithm-segmented one is higher than or equal to 0.75% for 90% of the images in the database. Average

[1]Results of the experiment for every image is available at [33], in the Optic Disc Results subsection of the Results section

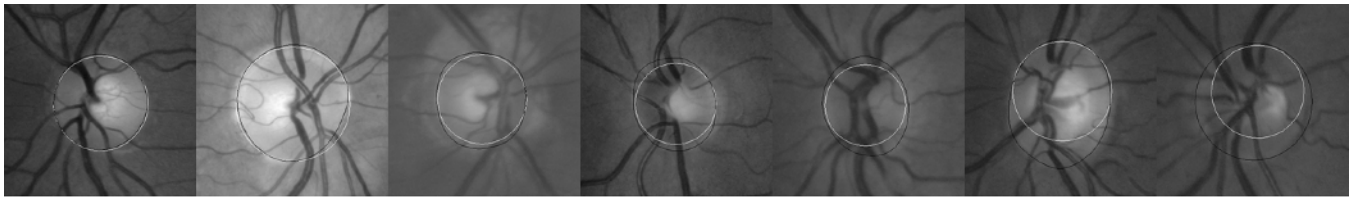

Fig. 4. Sample segmentations obtained with the presented methodology. (a) $S = 0.96$. (b) $S = 0.93$. (c) $S = 0.89$. (d) $S = 0.83$. (e) $S = 0.76$. (f) $S = 0.74$. (g) $S = 0.65$. White line: segmentations produced by the algorithm; black line: true OD areas labeled by specialists.

overlapping obtained for the whole set of images was 0.86. In this respect, note that the maximum overlapping reachable with a circular template-based approach is 0.92.

Fig. 4 shows segmentation examples obtained by the proposed methodology for all the overlapping intervals defined in Table I. It should be pointed out that, for segmentation algorithm testing, the location methodology presented in this paper was used to obtain the required initial OD location. This algorithm correctly found the OD in 1186 out of the 1200 images (99% success rate). OD location was manually determined in the 14 images in which the OD location algorithm failed.

The third row in Table I shows the performance results published by Lalonde *et al.* [21] for their circular template-based methodology. These results were obtained on a different database comprising 40 images taken from 27 patients attending a diabetic retinal-screening programme. As in the case of the MESSIDOR database, this set of images includes good, fair and bad visual quality images (Lalonde *et al.* considered bad quality images as those blurred and/or containing abnormally dark or bright regions). Our algorithm could not be tested on this database as we had no access to it. The algorithm proposed by Lalonde *et al.* (*Hausdorff-BasedTemplateMatching*) is based on minimizing the Hausdorff distance between previously obtained candidate edge map regions and a set of circular templates. As it can be observed, the *CircularHough* method exceeds the results of this methodology for all considered overlapping intervals and also enhances average overlapping.

Finally, tests concerning computational efficiency were also done. The tests were performed on a current midrange PC equipped with an Intel Core2Duo CPU at 2.13 GHz and 2 GB of RAM capacity. The algorithms were implemented in Java programming language and tested running on the Java Virtual Machine version 6. For a total of 1200 executions of the algorithm for OD segmentation, the average computational time obtained was 5.69 s. with a standard deviation of 0.54 s. The average computational time obtained for OD location was 1.67 s. with a standard deviation of 0.14 s.

V. Discussion on OD Segmentation Models

In this section, we discuss on the advantages and disadvantages of the most widely-used OD segmentation models: circular as well as elliptical template-based methods and deformable model-based methods. The first discussion focuses on the use of elliptical or circular models. For that, four different elliptical approaches were implemented and tested to compare them to the circular approximation presented here. In the second subsection, the proposed circular approach is compared to three deformable model-based algorithms and obtained results are discussed.

TABLE II
Comparison of Segmentation Potential of Different Models in Terms of Average Overlapping

	$\overline{S}$
Deformable Models	100%
Elliptical Template-Based Models	97%
Circular Template-Based Models	92%

A. The Presented Circular Template-Based Method Versus The Elliptical Template-Based Approach

According to OD shape features, the use of an elliptical model for OD segmentation, at least theoretically, should render higher segmentation potential. For empirical evaluation of this issue, the experiment used for circular model potential assessment was now reproduced and applied to elliptical models. That is, an "elliptical gold standard" set was generated by applying an elliptical model for fitting the true OD contours in the "gold standard" set of the database described in Section IV. So, the average overlapping of both sets may be considered the maximum segmentation potential of an elliptical model. Table II summarizes the potential of all models discussed in this section. As it can be observed, the use of an elliptical model renders a theoretical overlapping increase of 5% relative to the potential rendered by a circular model. Nevertheless, since the elliptical approach has two degrees-of-freedom more than the circular model (rotation angle and additional radius), its results may show a less robust and stable behavior.

To assess elliptical model behaviour, four elliptical template-based variants were implemented and applied to the I_{BM} obtained from operation (6). Three of these approaches were based on minimizing the algebraic distance [34], [35] and one was based on minimizing the geometric distance [34]. Each approach was tested on the database used in Section IV and results were measured using the metric defined in (9). Thus, the elliptical and circular approaches can be compared under the same conditions. Table III summarizes the results obtained in this test. Data are presented in columns as the percentage of images per interval of overlapping values, the penultimate column is the total average overlapping and the last one indicates the percentage of model-solved cases, as the tested methods do not always converge to a solution. The first row shows the results for the elliptical approach based on minimizing the geometric distance, the following three rows show the results obtained

TABLE III
COMPARISON BETWEEN THE PRESENTED CIRCULAR TEMPLATE-BASED METHOD AND FOUR ELLIPTICAL TEMPLATE-BASED APPROACHES. DATA IN TERMS OF PERCENTAGE OF IMAGES PER OVERLAPPING INTERVAL AND AVERAGE OVERLAPPING OF THE WHOLE SET

	$S \geq 0.95$	$S \geq 0.90$	$S \geq 0.85$	$S \geq 0.80$	$S \geq 0.75$	$S \geq 0.70$	$\overline{S}$	SF^*
EllipticalGeometricalMin [34]	2%	11%	20%	30%	39%	51%	0.67	89%
EllipticalAlgebraicMin1 [35]	2%	9%	17%	26%	36%	48%	0.66	99%
EllipticalAlgebraicMin2 [34]	2%	10%	19%	27%	36%	47%	0.65	87%
EllipticalAlgebraicMin3 [34]	2%	9%	18%	26%	35%	48%	0.66	98%
CircularHough (this work)	**7%**	**46%**	**73%**	**84%**	**90%**	**93%**	**0.86**	100%

* SF (Solutions Found): percentage of cases for which the model found a solution.

with the three variants based on minimizing the algebraic distance, and the last row show the results of the circular approach presented in this paper. Importantly, the average values for each elliptical method were calculated considering only the cases for which they had found a solution. Another important issue with regard to results is that no automated criterion was used for selecting for each image between the segmentations from the red and green channels. For each image, both candidates were measured and the one with the highest overlapping score was selected for method total average calculation. Hence, the results shown in Table III are the highest possible scores for each elliptical approach.

The results from this study indicate that the segmentation performance of all elliptical approaches is similar. The greater difference between them was observed at the percentage of solved cases. Interestingly, their performance is significantly poorer than that obtained with the circular model. This performance degradation is the result of elliptical models's higher sensitivity to poor OD border contrast and, therefore, to poor border extraction. These models require the extraction of a great amount of OD representative borders to provide correct estimations of the two radiuses and rotation angle. On the other hand, the circular model proposed in this paper only needs some portions of the OD contour to obtain a fitting circumference. Although the preprocessing designed in this work may not be the most appropriate for elliptical models, their direct application for OD segmentation is suggested here to offer less stable and homogeneous behavior.

B. The Presented Circular Template-Based Method Versus the Deformable Model-Based Approach

The main advantage of using a deformable model instead of a template-based model for OD segmentation is that, theoretically, 100% of overlapping areas between the automated segmentation and the ground truth may be achieved. As shown in Table II, it involves an 8% increase relative to a circular model. This is why deformable models have much more degrees-of-freedom than template-based models to fit the desired shape. However, these additional freedom degrees-of-freedom make these models more sensitive to irregular or low OD boundary contrast.

As a basis for this discussion, the template-based method proposed here was compared to the three OD segmentation approaches based on deformable models proposed by Lowell *et al.* in [18]. For the sake of comparison rigorousness, we used the same database, "gold standard" set and metric as those used in this work. Thus, the algorithms can be compared under identical

TABLE IV
COMPARISON BETWEEN THE PRESENTED CIRCULAR TEMPLATE-BASED METHOD AND THREE DEFORMABLE MODEL-BASED APPROACHES IN TERMS OF PERCENTAGE OF IMAGES PER SUBJECTIVE CATEGORY

	Excellent	Good	Fair	Poor	Excellent-Fair
CircularHough	**40%**	**39%**	**18%**	**3%**	**97%**
TemporalLock [18]	42%	31%	10%	17%	83%
DV-Hough [18]	39%	22%	20%	19%	81%
Simple [18]	9%	8%	30%	53%	47%

conditions. The database is composed of 90 images acquired at a resolution of 640×480 and 8 bits per color plane. These images were taken from 50 patients, 19 of them being affected by type 2 diabetes mellitus; the diabetes status was unavailable for the remaining 31. To produce the "gold standard" segmentation for this set of images, four clinicians manually delimited the rim for each image, and the mean and radial standard deviations of these contours were calculated. Then, Lowell *et al.* defined the discrepancy δ^j as

$$\delta^j = \sum_i \frac{m_i^j - \mu_i^j}{\sigma_i^j - \epsilon} \tag{10}$$

where μ_i^j and σ_i^j summarize the clinicians choice of rim location on spoke i of image j and m_i^j is segmentation location on spoke i for image j. Spokes are points belonging to the OD rim; 24 spokes were considered taken each 15°. Division by σ compensates for uncertainty in rim position and ϵ is a small factor to prevent division by zero where the clinicians are in exact agreement. In addition to this measure, they defined four categories corresponding to their subjective perception of quality. These four categories are *Excellent*, *Good*, *Fair*, and *Poor*, referencing images with disparity up to one, two, five, or more, respectively. They assessed their algorithms performance considering the percentage of segmentations classified in the range *Excellent–Fair*.

Table IV summarizes the performance on this subjective scale for their three alternative algorithms and the one proposed in this paper. Results are expressed in terms of the percentage of images per subjective category. As it can be observed, with the best deformable model approach, 2% more of excellent segmentations were obtained than with the presented approach. Nevertheless, the template-based approach provided a significant enhancement in the percentage of obtained "valid" segmentations, thus reaching the 79% versus 73% of segmentations within the *Excellent–Good* range, and 97% versus 83% of segmentations within the *Excellent–Fair* range.

The results of this experiment, in spite of not being applicable to all template-based and deformable models, are a good example of comparable segmentation performance of both approaches on a particular common case. Therefore, the main conclusion of this experiment would be that, for OD segmentation, under appropriate OD background-contrast conditions, deformable models render more accurate OD segmentations. On the contrary case, when contrast conditions are not so favourable, the circular approach may turn out to be a more robust and reliable solution.

VI. Discussion and Conclusion

This paper presents a new template-based approach for OD segmentation by means of a circular OD-boundary approximation. In addition, an OD location methodology for obtaining the OD position needed by the segmentation algorithm as initial information is also proposed.

The results presented in this paper show that the proposed methodology offers a reliable and robust solution for OD segmentation. According to the results in Table I, the overlapping between the "true" OD region and the one segmented by our algorithm is over 0.75 in 90% of the 1200 MESSIDOR images, being the average overlapping 0.86 for the whole set of images. This result is more valuable taking into account that maximum overlapping with a circular template-based approach is 0.92. Referentially, it can be pointed out that performance comparisons with the circular template-based approach by Lalonde *et al.* [21] show that the overlapping obtained by our proposal was clearly higher, in spite of the fact that our results were obtained on a set of 1200 images while Lalonde *et al.* used only 40 (results are shown in Table I).

Moreover, discussion in Section V on different OD segmentation, strengthens the hypothesis of the suitability of circular models for this purpose. The tests summarized in Table II indicate that the overlapping area between ground-truth OD segmentations and those obtained by elliptical models is higher than those obtained by circular models (97% and 92%, respectively). However, when testing with numerous and different real cases, the simplicity of the presented circular model generally favours obtaining a more robust behaviour. Thus, performance comparisons between the proposed circular template-based method and four elliptical template-based approaches for the MESSIDOR images (Table III) indicate that the circular approach renders a clearly higher average overlapping. The same conclusion was drawn for deformable models. Although these models can theoretically obtain 100% overlapping, the performance results presented in terms of discrepancy grades in Table IV, indicate that our proposed circular model outperforms the deformable model proposed by Lowell *et al.* in [18].

On the other hand, it must be mentioned that, to facilitate performance comparison between OD segmentation methods, the generated hand segmentations of the OD rim for the 1200 images in the MESSIDOR database are currently available for researchers at [33], in the Sample Databases subsection within the Results section by selecting the MESSIDOR database. The original database is available at [32]. To the best of our knowledge, such a set of "gold standard" images from a clinically labelled database is not available for the research community at the present time.

The main conclusions of this work can be summarized as follows.

1) The performance results obtained by the proposed methodology on a huge digital retinal database indicate that simple methods, based on basic image processing techniques, seem to suffice for OD location and segmentation.
2) A circular modelling for the OD boundary, compared to elliptical and deformable models, was shown to offer good compromise between success rate, quality and efficiency, as shown by comparing its segmented area to experts' free-drawn areas.

Despite all of this, the existence of some specific cases in which, due to their exceptional ellipsity degree, the circular approach does not reach the performance results of the elliptical approach has been reported [see, for instance, the case in Fig. 4(f)]. With the aim of enhancing the overlapping rates obtained in this work for these isolated cases, the authors' current research is focused on the development of a methodology for performing a controlled elliptical deformation of the obtained circumference. Within the framework of this study, whether any preprocessing modification is necessary or even whether postprocessing would be appropriate for assuring deformation process stability is currently under study.

Acknowledgment

The authors would like to thank the Messidor program partners for facilitating their database. Special thanks to Dr. A. Hunter for his generosity, as he provided us with the material which made possible the study presented in Section V-A.

References

[1] H. R. Taylor and J. E. Keeffe, "World blindness: A 21st century perspective," *Br. J. Ophthalmol.*, vol. 85, pp. 261–266, 2001.
[2] S. Wild, G. Roglic, A. Green, R. Sicree, and H. King, "Global prevalence of diabetes: Estimates for the year 2000 and projections for 2030," *Diabetes Care*, vol. 27, pp. 1047–1053, 2004.
[3] D. Klonoff and D. Schwartz, "An economic analysis of interventions for diabetes," *Diabetes Care*, vol. 23, pp. 390–404, 2000.
[4] N. Patton, T. M. Aslam, T. MacGillivray, I. J. Deary, B. Dhillon, R. H. Eikelboom, K. Yogesan, and I. J. Constable, "Retinal image analysis: Concepts, applications and potential," *Prog. Retin. Eye Res.*, vol. 25, pp. 99–127, 2006.
[5] A. Singalavanija, J. Supokavej, P. Bamroongsuk, C. Sinthanayothin, S. Phoojaruenchanachai, and V. Kongbunkiat, "Feasibility study on computer-aided screening for diabetic retinopathy," *Jpn. J. Ophthalmol.*, vol. 50, pp. 361–366, 2006.
[6] C. Sinthanayothin, J. F. Boyce, H. L. Cook, and T. H. Williamson, "Automated localisation of the optic disc, fovea, and retinal blood vessels from digital colour fundus images," *Br. J. Ophthalmol.*, vol. 83, pp. 902–910, 1999.
[7] H. Li and O. Chutatape, "Automatic location of optic disc in retinal images," in *Proc. IEEE Int. Conf. Image Process.*, 2001, pp. 837–840.
[8] L. Gagnon, M. Lalonde, M. Beaulieu, and M. C. Boucher, "Procedure to detect anatomical structures in optical fundus images," in *Proc. Conf. Med. Imag. 2001: Image Process.*, San Diego, CA, 2001, pp. 1218–1225.
[9] A. Osareh, M. Mirmehdi, B. Thomas, and R. Markham, "Automated identification of diabetic retinal exudates in digital colour images," *Br. J. Ophthalmol.*, vol. 87, pp. 1220–1223, 2003.
[10] H. A. Quigley and A. T. Broman, "The number of people with glaucoma worldwide in 2010 and 2020," *Br. J. Ophthalmol.*, vol. 90, pp. 262–267, 2006.

[11] H. Li and O. Chutatape, "A model-based approach for automated feature extraction in fundus images," in *Proc. 9th IEEE Int. Conf. Comput. Vis. (ICCV'03)*, 2003, vol. 1, pp. 394–399.

[12] C. Sinthanayothin, "Image analysis for automatic diagnosis of diabetic retinopathy," Ph.D. dissertation, Univ. London, London, U.K., 1999.

[13] A. Hoover and M. Goldbaum, "Locating the optic nerve in a retinal image using the fuzzy convergence of the blood vessels," *IEEE Trans. Med. Imag.*, vol. 22, no. 8, pp. 951–958, Aug. 2003.

[14] A. Hoover and M. Goldbaum, "Fuzzy convergence," in *Proc. IEEE Comput. Soc. Conf. Comput. Vis. Pattern Recognit.*, Santa Barbara, CA, 1998, pp. 716–721.

[15] M. Foracchia, E. Grisan, and A. Ruggeri, "Detection of optic disc in retinal images by means of a geometrical model of vessel structure," *IEEE Trans. Med. Imag.*, vol. 23, no. 10, pp. 1189–1195, Oct. 2004.

[16] A. A. H. A. R. Youssif, A. Z. Ghalwash, and A. R. Ghoneim, "Optic disc detection from normalized digital fundus images by means of a vessels' direction matched filter," *IEEE Trans. Med. Imag.*, vol. 27, pp. 11–18, 2008.

[17] A. Osareh, M. Mirmehdi, B. Thomas, and R. Markham, "Comparison of colour spaces for optic disc localisation in retinal images," in *Proc. 16th Int. Conf. Pattern Recognit.*, 2002, pp. 743–746.

[18] J. Lowell, A. Hunter, D. Steel, A. Basu, R. Ryder, E. Fletcher, and L. Kennedy, "Optic nerve head segmentation," *IEEE Trans. Med. Imag.*, vol. 23, no. 2, pp. 256–264, Feb. 2004.

[19] J. Xu, O. Chutatape, E. Sung, C. Zheng, and P. C. T. Kuan, "Optic disk feature extraction via modified deformable model technique for glaucoma analysis," *Pattern Recognit.*, vol. 40, no. 7, pp. 2063–2076, 2007.

[20] D. W. K. Wong, J. Liu, J. H. Lim, X. Jia, F. Yin, H. Li, and T. Y. Wong, "Level-set based automatic cup-to-disc ratio determination using retinal fundus images in ARGALI," in *Proc. 30th Annu. Int. IEEE EMBS Conf.*, 2008, pp. 2266–2269.

[21] M. Lalonde, M. Beaulieu, and L. Gagnon, "Fast and robust optic disk detection using pyramidal decomposition and Hausdorff-based template matching," *IEEE Trans. Med. Imag.*, vol. 20, no. 11, pp. 1193–1200, Nov. 2001.

[22] T. Walter and J. C. Klein, "Segmentation of color fundus images of the human retina: Detection of the optic disc and the vascular tree using morphological techniques," in *Proc. 2nd Int. Symp. Med. Data Anal.*, 2001, pp. 282–287.

[23] A. W. Reza, C. Eswaran, and S. Hati, "Automatic tracing of optic disc and exudates from color fundus images using fixed and variable thresholds," *J. Med. Syst.*, vol. 33, pp. 73–80, 2008.

[24] M. D. Abràmoff, W. L. M. Alward, E. C. Greenlee, L. Shuba, C. Y. Kim, J. H. Fingert, and Y. H. Kwon, "Automated segmentation of the optic disc from stereo color photographs using physiologically plausible features," *Invest. Ophthalmol. Vis. Sci.*, vol. 48, no. 4, pp. 1665–1673, 2007.

[25] T. Walter and J. C. Klein, "Automatic analysis of color fundus photographs and its application to the diagnosis of diabetic retinopathy," in *Handbook of Biomedical Image Analysis*. New York: Kluwer, 2005, vol. 2, pp. 315–368.

[26] N. Otsu, "A threshold selection method from gray-scale histogram," *IEEE Trans. Syst. Man Cybern.*, vol. 8, pp. 62–66, 1978.

[27] C. Heneghan, J. Flynn, M. O'Keefe, and M. Cahill, "Characterization of changes in blood vessel width and tortuosity in retinopathy of prematurity using image analysis," *Med. Image Anal.*, vol. 6, pp. 407–429, 2002.

[28] R. C. Gonzalez and R. E. Woods, "Image Segmentation," in *Digital Image Processing*, 2nd ed. Upper Saddle River, NJ: Prentice-Hall, 2002, pp. 577–581.

[29] P. V. C. Hough, "Methods and means for recognizing complex patterns," U.S. Patent 3 069 654, Dec. 1962.

[30] R. O. Duda and P. E. Hart, "Use of the Hough transformation to detect lines and curves in picture," *Commun. ACM*, vol. 15, pp. 11–15, 1972.

[31] C. Kimme, D. Ballard, and J. Sklansky, "Finding circles by an array of accumulators," *Commun. Assoc. Comput. Mach.*, vol. 18, pp. 120–122, 1975.

[32] *Download Images Section, MESSIDOR: Digital Retinal Images, MESSIDOR TECHNO-VISION Project, France*, [Online]. Available: http://messidor.crihan.fr/download-en.php

[33] Expert system for early automated detection of DR by analysis of digital retinal images project website. Huelva, Spain, Univ. Huelva [Online]. Available: http://www.uhu.es/retinopathy

[34] W. Gander, G. H. Golub, and R. Strebel, "Least square fitting of circles and ellipses," *BIT*, no. 43, pp. 558–578, 1994.

[35] A. Fitzgibbon, M. Pilu, and R. B. Fisher, "Direct least square fitting of ellipses," *IEEE Trans. Pattern Anal. Mach. Intell.*, vol. 21, no. 5, pp. 476–480, May 1999.

Detecting the Optic Disc Boundary in Digital Fundus Images Using Morphological, Edge Detection, and Feature Extraction Techniques

Arturo Aquino*, Manuel Emilio Gegúndez-Arias, and Diego Marín

***Abstract*—Optic disc (OD) detection is an important step in developing systems for automated diagnosis of various serious ophthalmic pathologies. This paper presents a new template-based methodology for segmenting the OD from digital retinal images. This methodology uses morphological and edge detection techniques followed by the Circular Hough Transform to obtain a circular OD boundary approximation. It requires a pixel located within the OD as initial information. For this purpose, a location methodology based on a voting-type algorithm is also proposed. The algorithms were evaluated on the 1200 images of the publicly available MESSIDOR database. The location procedure succeeded in 99% of cases, taking an average computational time of 1.67 s. with a standard deviation of 0.14 s. On the other hand, the segmentation algorithm rendered an average common area overlapping between automated segmentations and true OD regions of 86%. The average computational time was 5.69 s with a standard deviation of 0.54 s. Moreover, a discussion on advantages and disadvantages of the models more generally used for OD segmentation is also presented in this paper.**

***Index Terms*—Diabetic retinopathy, glaucoma, optic disc (OD) segmentation, retinal imaging, telemedicine.**

I. Introduction

DIABETIC retinopathy (DR) is a chronic disease which nowadays constitutes the primary cause of blindness in people of working age in the developed world [1]–[3]. The benefits that a system for automaticly detect early signs of this disease would provide have been widely studied and assessed positively by experts [4], [5]. In this sense, the OD plays an important role in developing automated diagnosis expert systems for DR as its segmentation is a key preprocessing component in many algorithms designed to identify other fundus features. The relatively constant distance between the OD and the fovea, can be used to help estimate the location of the latter [6]. On the other hand, to segment the vascular tree, vessel tracking methods need an initial seed vessel point. For this, pixels of vessels within the OD or in its vicinity have been used [7], [8]. In addition, OD segmentation can be useful in diagnosing automatically some diseases caused by DR. Finding the OD can be used to decrease false positives in the detection of regions of retinal exudates [9]. These injuries are a diagnostic key to grading the risk of macular edema.

OD segmentation is also relevant for automated diagnosis of other ophthalmic pathologies. One of them and maybe the most noteworthy is Glaucoma. It is the second most common cause of blindness worldwide [10]. Glaucoma is identified by recognizing the changes in shape, color, or depth that it produces in the OD [11]. Thus, its segmentation and analysis can be used to detect evidence of Glaucoma automatically.

The OD can be distinguished in eye fundus images as a slightly elliptical shape. Its size may vary significantly and different estimations have been made. Whereas Sinthanayothin *et al.* [6] stated that it occupies about one-seventh of the entire image, alternatively other authors have pointed out that OD size varies from one person to another, occupying about one-tenth to one-fifth of the image [7]. In color fundus images, the OD usually appears as a bright yellowish region, although this feature may also experience significant variations (Fig. 1).

OD segmentation is not an easy matter. Besides the variations in OD shape, size, and color pointed out previously, there are some additional complications to take into account. Contrast all around the OD boundary is usually not constant or high enough piecewise due to outgoing vessels that partially obscures portions of the rim producing "shadows." Another distractor is produced when peripapillary atrophy is present, as this produces bright areas just outside the OD rim which distort its shape. On the other hand, eye movement at the moment of retinography capture may also lead to slightly blurred images, making their automated analysis even more difficult. This problem can be avoided by simply discarding these images and retaking new ones. However, this method is not usually applied as their quality is usually good enough for human visual inspection.

This paper presents a new template-based method for OD segmentation. Firstly, an OD-containing sub-image is extracted: an OD pixel and its surrounding region (a surrounding region wide enough to include the whole OD) are selected. With this purpose, an OD location methodology is also proposed here. Then,

Manuscript received April 05, 2010; revised May 25, 2010; accepted June 05, 2010. This work is part of the Expert System for Early Automated Detection of DR by Analysis of Digital Retinal Images Project, supported and funded by the Health Ministry of the Andalusian Regional Government (Spain). *Asterisk indicates corresponding author.*

*A. Aquino is with the Department of Electronic, Computer Science and Automatic Engineering, "La Rábida" Polytechnic School, University of Huelva, 21071 Huelva, Spain (e-mail: arturo.aquino@diesia.uhu.es).

D. Marín is with the Department of Electronic, Computer Science and Automatic Engineering, "La Rábida" Polytechnic School, University of Huelva, 21071 Huelva, Spain (e-mail: diego.marin@diesia.uhu.es).

M. E. Gegúndez-Arias is with the Department of Mathematics, "La Rábida" Polytechnic School, University of Huelva, 21071 Huelva, Spain (e-mail: gegundez@uhu.es).

Color versions of one or more of the figures in this paper are available online at http://ieeexplore.ieee.org.

Digital Object Identifier 10.1109/TMI.2010.2053042

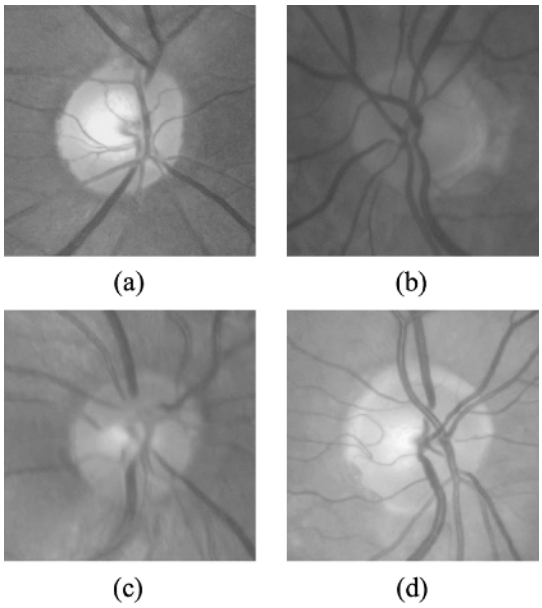

Fig. 1. Examples of OD appearance. (a) Yellowish OD. (b) Brownish OD. (c) Reddish OD. (d) Whitish OD.

the OD boundary is extracted in parallel from both the red and green channels of this sub-image by means of morphological and edge detection techniques. Both OD boundaries are approximated by a circumference using the Circular Hough Transform. The "better" of these results is finally selected. This paper also includes a study on advantages and disadvantages involved by the use of circular, elliptical and deformable models for OD segmentation. The results of this study strengthen the hypothesis of the suitability of circular models for this purpose and show evidence that the circular approach offers good compromise between success rate, quality, and efficiency.

II. Overview of State of Art

The available works related to OD processing in eye fundus color images can be grouped into two distinct categories: *location* and *segmentation* methods. The former works focus on finding an OD pixel (generally representative of its center). On the other hand, the latter works estimate the OD boundary. Within this category, a general distinction can be made between *template-based* methods (methods for obtaining OD boundary approximations) and methods based on *deformable models* or *snakes* for extracting the OD boundary as exactly as possible. With regard to location methods, Synthanayothin *et al.* presented a method [6], [12] where the images were preprocessed by applying an adaptative local contrast enhancement to the intensity channel of the HSI color space. The OD center location was identified using the variance of intensity produced by the blood vessels within the OD. Hoover and Goldbaum [13], [14] located the center of the OD using the vasculature origin. They determined where all the vessels converged by means of a voting-type algorithm called fuzzy convergence. Another method that uses the convergence of the vessels to detect the OD center was proposed by Foracchia *et al.* [15]. The four main vessels originating from the OD were geometrically modeled using two parabolas, and the OD position was located as their common vertex. Inspired by previous works, Youssif *et al.* [16] presented an OD location method based on a vessels' direction matched filter. As a first step a binary mask was generated followed by image brightness and contrast equalization. Finally, the retinal vasculature was segmented, and the directions of the vessels were matched to the proposed filter representing the expected vessels' directions in the vicinity of the OD.

With regard to segmentation methods and concretely to works based on deformable models, Osareh *et al.* [17] located the OD center by means of template matching and extracted its boundary using a snake initialized on a morphologically enhanced region of the OD. Lowell *et al.* [18] also localized the OD by means of template matching as well as also selected a deformable contour model for its segmentation. Specifically, they used a global elliptical model and a local deformable model with variable edge-strength dependent stiffness. Another deformable model-based approach was presented in [19]. The snake behavior against vessel occlusion was improved and the model was extended in two aspects: knowledge-based clustering and smoothing update. Thus, the snake deformed to the location with minimum energy and then self-clustered into two groups, which were finally updated by the combination of both local and global information. Regarding template-based methods, Wong *et al.* [20] proposed: 1) OD location by means of histogram analysis and initial contour definition according to the previously obtained location, and 2) a modified version of the conventional level-set method was subsequently used for OD boundary extraction from the red channel. This contour was finally fitted by an ellipse. Another template-matching approach for OD segmentation is the Hausdorff-based template matching presented by Lalonde *et al.* [21]. Initially, they determined a set of OD candidate regions by means of multiresolution processing through pyramidal decomposition. For each OD region candidate, they calculated a simple confidence value representing the ratio between the mean intensity inside the candidate region and inside its neighborhood. The Canny edge detector and a Rayleigh-based threshold were then applied to the green-band image regions corresponding to the candidate regions, constructing a binary edge map. As final step, using the Hausdorff distance between the edge map regions and circular templates with different radii, they decided the OD among all the candidates. On the other hand, although they do not belong to the two reviewed categories, works [22]–[24] proposed other relevant OD segmentation methods. Walter and Klein [22] found the OD contour through the watershed transformation. For OD detection, its center was previously approximated as the centroid of the largest and brightest connected object in a binary image obtained by thresholding the intensity channel. Reza *et al.* [23] also used the watershed transformation for OD segmentation. Firstly, the green channel was preprocessed for image condition enhancement. Then, morphological opening, extended maxima operator and minima imposition were finally used to apply the watershed transformation for bright structure segmentation. Finally, although applied to stereo images, it is worth mentioning the novel OD segmentation approach presented by Abràmoff *et al.* [24]. Pixel feature classification by means of a k-nearest neighbor classifier was used in this case for OD segmentation in stereo color photographs.

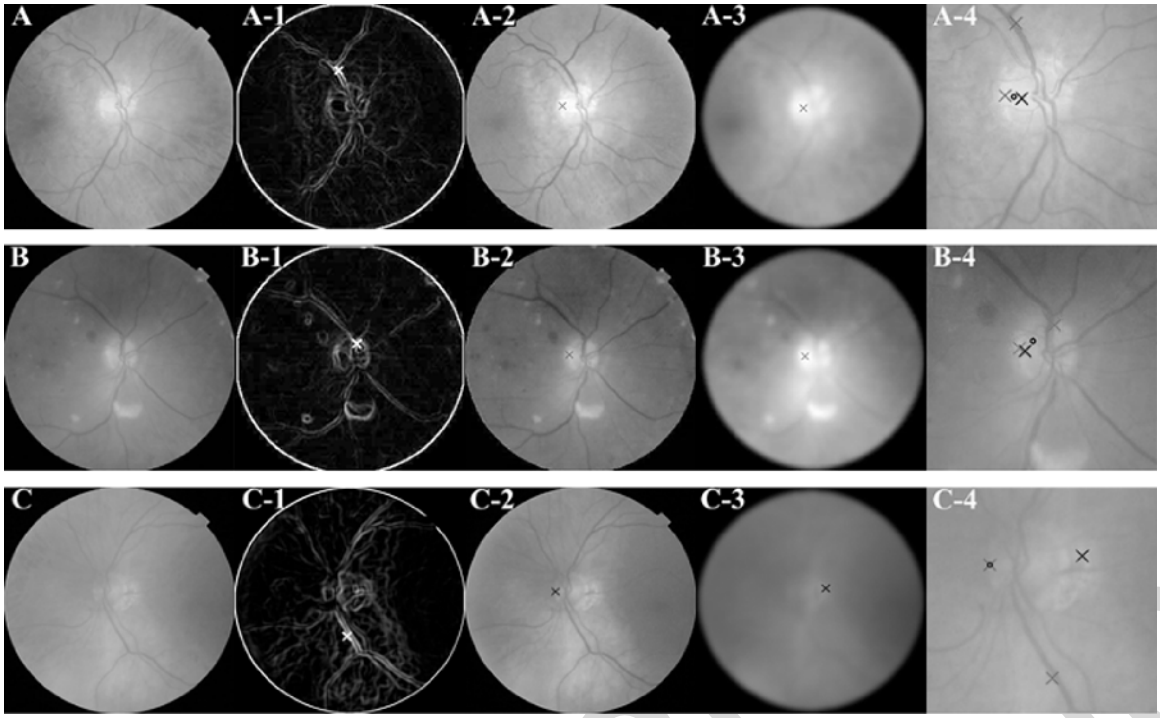

Fig. 2. ODP determination: (A), (B), and (C) Original images. (A-1), (B-1), and (C-1) OD pixels rendered by the maximum difference method. (A-2), (B-2), and (C-2) OD pixels rendered by the maximum variance method. (A-3), (B-3), and (C-3) OD pixels rendered by the low-pass filter method. (A-4), (B-4), and (C-4) Final ODP determination (black circumference): in (A-4), although the OD pixel of the maximum difference method is not properly selected, the ODP is successfully located; in (B-4) the ODP selected is the centroid of the three OD pixels; in (C-4), since the three OD pixels are far from their centroid, the ODP selected is the OD pixel from the maximum variance method.

III. Methodology

The aim of this work is to introduce a new methodology for OD segmentation that obtains a circular boundary approximation. It needs as initial information the coordinates of a pixel located within the OD. To this effect, in order to complement the presented segmentation methodology, a simple but reliable and very fast OD location methodology is also proposed to obtain the required OD pixel. It must be stressed that any other location method could be used for this purpose.

All values of parameters, constants and window sizes given in this section refer to retinas of 1046 pixels in diameter. For different image resolutions, all of these values would have to be scaled.

A. Optic Disc Location

The location methodology obtains a pixel [called Optic Disc Pixel (ODP)] that belongs to the OD. It comprises three independent detection methods. Each method obtains its own OD candidate pixel. The final ODP is selected by taking into account the three previous candidate pixels and their location with respect to their average point (centroid). For this, a voting procedure comprising the following cases is applied.

- If the three OD candidate pixels are close to the centroid (closer than one-fifth of the image, maximum OD diameter estimation [7]): the selected ODP is the centroid.
- If only two candidates are close to the centroid: the selected ODP is the average point in these two referred pixels.
- Otherwise, the selected ODP is the candidate pixel obtained with the most reliable method (performed tests show this is the maximum variance method described below).

The three developed methods work on the green channel of the RGB color space as this is the one that provides the best contrast [25]. This gray scale image will be denoted as I. A description of these methods, illustrated in Fig. 2 by three examples of their application to different eye fundus images, is presented as follows.

- Maximum Difference Method: The OD usually appears as a bright region in eye fundus images. Moreover, the vascular tree formed by the "dark" blood vessels emerges in the disc. This is why the maximum variation of the gray levels usually occurs within the OD. This maximum is used by this method to select its OD pixel.
  A median filter of 21×21 is applied beforehand to I in order to remove nonsignificant peaks in the image. If I_M denotes this filtered image, the OD pixel from this method is decided according to the following equation:
  $$P_{\mathrm{MDM}} = \arg\limits_{(i,j)} \left(\max \left\{ (I_M)_W^{\mathrm{MAX}}(i,j) - (I_M)_W^{\mathrm{MIN}}(i,j) \right\} \right) \quad (1)$$
  where $(I_M)_W^{\mathrm{MAX}}$ and $(I_M)_W^{\mathrm{MIN}}$ are, respectively, the maximum and the minimum values of the pixels in I_M within a window W of size 21×21 centered on a pixel (i,j) (see examples in Fig. 2, images A-1, B-1, and C-1).
- Maximum Variance Method: This method is based on the same properties as the previous one. It calculates the statistical variance for every pixel by using a 71×71 centered

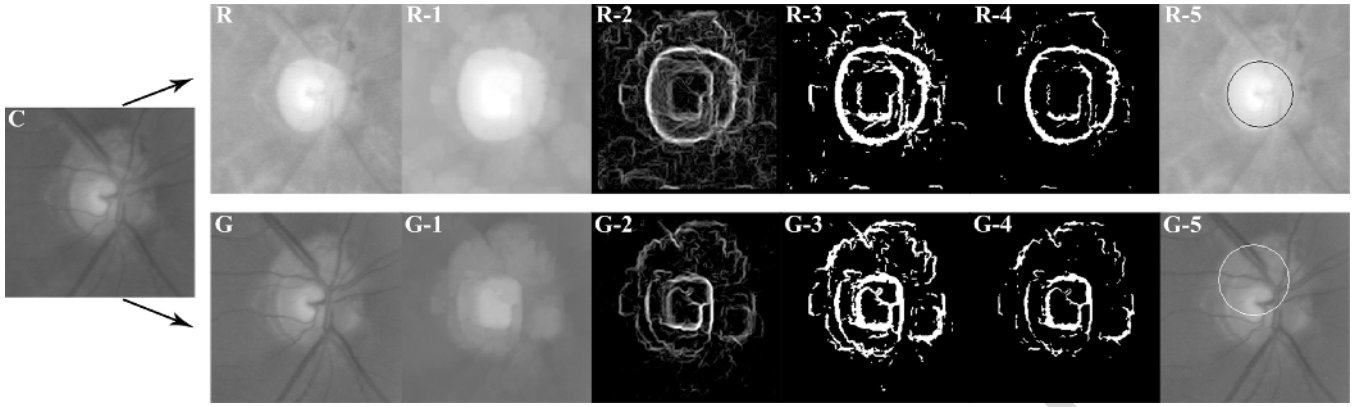

Fig. 3. Illustration of the process for the calculation of the circular OD boundary approximation: (C) Initial RBG sub-image containing an OD affected by peripapillary atrophy. On the right, the top row shows the process performed on the red channel, whereas the bottom corresponds to the process applied to the green component. (R) and (G) Subimages extracted from the red and green channels of (C), respectively. (R-1) and (G-1) Vessel elimination. (R-2) and (G-2) Gradient magnitude image. (R-3) and (G-3) Binary image. (R-4) and (G-4) Cleaner version of the binary image. (R-5) and (G-5) Circular OD boundary approximation. The scores obtained in the Circular Hough Transform algorithm are, 264 for segmentation in (R-5) and 130 for segmentation in (G-5), so the segmentation selected would be the one performed on the red channel.

window. On the other hand, a set of "bright" pixels is obtained by automatic blue-channel thresholding according to the Otsu method [26]. The OD pixel returned by this method is the maximum variance pixel showing at least 10 "bright" pixels in its neighborhood (established by means of a 101×101 pixel window) (see Fig. 2, images A-2, B-2, and C-2). The window sizes selected to compute the variance and to establish the neighborhood criteria, were set with the aim of obtaining the best location performance on a set of 1200 fundus images (this database is described in Section IV).

- Low-Pass Filter Method: The OD pixel of this method is the maximum gray-level pixel in a low-pass filtered image. Although the OD is usually the brightest area in a retinography, the pixel with the highest gray level could not be located within it. In many cases, this pixel may be inside other small bright regions. In order to smooth out these distractors, the image I is transformed to the frequency domain and filtered by the Gaussian low-pass filter defined as follows:

$$H(u,v) = \exp\left(\frac{-D^2(u,v)}{2D_0^2}\right) \tag{2}$$

where $D(u,v)$ is the Euclidean distance between the point (u,v) and the origin of the frequency plane, and D_0 is the cutoff frequency with a value of 25 Hz. The highest gray-level pixel in the filtered image returned to the spatial domain is the result of this method (Fig. 2, images A-3, B-3, and C-3).

The result of the final ODP selection process is illustrated by the three examples of application of the methodology shown in Fig. 2. In the first example (Fig. 2, images A to A-4), it can be confirmed that although the pixel returned by the maximum difference method is outside the disc, it is discarded and the ODP is successfully selected. In the second example (Fig. 2, images B to B-4), pixels returned by the three methods are close, so the location of the ODP is the location of their centroid. In the last example (Fig. 2, images C to C-4), the three partial results are far from their centroid, so the final ODP is the OD pixel found by the maximum variance method.

B. Optic Disc Boundary Segmentation

The method proposed in this paper is performed on an RGB sub-image of the original retinography. By this way, robustness and efficiency in OD segmentation are increased as it reduces the search space and decreases the number of artifacts and distractors present in the whole image. So, as a first step, a 400×400 RGB sub-image is extracted centered on an OD pixel provided by the OD location methodology previously presented, or by any other if desired.

Although the green component of an RGB retinography is the one with highest contrast [25], the OD is often present in the red field as a well-defined white shape, brighter than the surrounding area. When contrast between the OD shape and its environment in this color field is high enough, the OD can usually be segmented better than in the green field. At other times, the OD is not discernable in the red component and has to be segmented in the green one. To exploit this feature, the OD segmentation is performed in parallel on the two components and the "better" of the two segmentations is ultimately selected. The proposed procedure firstly employs an special morphological processing to eliminate blood vessels. Then, a binary mask of the OD boundary candidates is obtained by applying edge detection and morphological techniques. Finally, the Circular Hough Transform is used to calculate the circular approximation of the OD.

1) Elimination of Blood Vessels: Consider the gray-level image I from the red or green field of the sub-image containing the OD (Fig. 3, images R and G). As was discussed, blood vessels within the OD act as strong distractors, so they should be erased from the image beforehand. The vasculature is piecewise linear and can be considered as a structure composed of many such connected linear shapes with a minimum length L and a maximum width W, where usually $W \ll L$ (see Heneghan *et al.* [27]). These linear shapes are formed, as a general rule, by a set of pixels with an almost constant gray-level value, with

this value being somewhat lower than the gray-level values of non-vessel pixels in their vicinity. Using a rotating linear structuring element B of width 1 and length $L_1 \gg W$, a linear shape can be detected by calculating the statistical variance of gray-level values of pixels along it. The rotation associated with the minimum value will be that in which the vessel contains B and, conversely, the rotation with the highest value will refer to the situation in which B crosses the linear shape. Thus, vessels can be removed from image I by finding, for every pixel, the rotation which produces the maximum gray level variance value and taking the maximum gray-level in the neighborhood defined by the structuring element at that rotation (see effects at Fig. 3, images R-1 and G-1). Mathematically this can be expressed as

$$I_{\neg V}(i,j) = I_{B_r}^{\mathrm{MAX}}(i,j) \tag{3}$$

where

$$r = \arg_k \left(\max \left\{ I_{B_k}^{\mathrm{VAR}}(i,j),\ k = 1, \ldots, 12 \right\} \right) \tag{4}$$

B_r represents structuring element B at rotation r determined by (4). Twelve rotations of the structuring element each 15° apart were used. The length L_1 of the structuring element should be chosen so as to cross vessels in order to erase them by applying (3). Taking into account the study proposed by Heneghan *et al.* in [27], the value for this parameter was set to 27. This operation produces an OD enlargement of L_1 pixels in all directions. This will be considered at the end of the processing.

2) Obtaining Od Boundary Candidates: The OD boundary represents the frontier between the OD and the background. It is characterized by a sudden variation in gray levels, with these values higher within the OD than in its surroundings. So, the OD boundary can be detected by measuring the gradient magnitude of gray-level changes in small neighborhoods of the image. Firstly, a mean filter is applied to eliminate pixel values unrepresentative of their environment. Then, the Prewitt edge detector [28] is used to obtain a gradient magnitude image (hereafter I_{GM}). This operator estimates image edge and orientation by convolving two 3×3 kernels which approximate derivatives for horizontal and vertical changes. The gradient magnitude image is finally obtained by taking the module of partial derivative values for every pixel. Thus, I_{GM} is an image which contains information on edges, specifically on the location and intensity of local gray-level variations (Fig. 3, images R-2 and G-2). As the blood vessels were previously erased, in general the most significant edges in the gradient image correspond to the OD boundary. Thus, a binary mask of OD boundary candidates can be produced by thresholding the image I_{GM}.

As stated before, there is great variability in OD appearance, and the contrast level between the OD and the background may vary quite substantially. That is why it is not suitable to establish a unique threshold for any image. The Otsu thresholding method [26] automatically decides a threshold for a gray-level image by assuming that it is composed of two sets, the background and the foreground. Then, the method establishes the optimum threshold T_{OTSU} by maximizing the between-class variance. Using this threshold, a first binary mask of OD boundary candidates is given by a simple binarization operation (see Fig. 3, images R-3 and G-3)

$$I_B(i,j) = \begin{cases} 0, & \text{if } I_{\mathrm{GM}}(i,j) \leq T_{\mathrm{OTSU}} \\ 255, & \text{if } I_{\mathrm{GM}}(i,j) > T_{\mathrm{OTSU}}. \end{cases} \tag{5}$$

This image can contain some noise caused by small rims present in the original image and detected in I_{GM}. So, the definitive binary mask of OD boundary candidates is obtained by cleaning I_B by means of morphological erosion (Fig. 3, images R-4 and G-4),

$$I_{\mathrm{BM}}(i,j) = (I_B)_C^{\mathrm{MIN}}(i,j) \tag{6}$$

where C is a circular structuring element with a diameter of five pixels. This operation reduces the OD radius in two pixels.

3) Final OD Boundary Segmentation: The Hough Transform [29] is widely used in Computer Vision and Pattern Recognition for detecting geometrical shapes that can be defined by parametric equations. Based on the primitive Hough Transform [29], the Circular Hough Transform was outlined by Duda *et al.* [30] and later improved and extended by Kimme *et al.* [31]. It aims to find circular patterns within an image. It is used to transform a set of feature points in the image space into a set of accumulated votes in a parameter space. Then, for each feature point, votes are accumulated in an accumulator array for all parameter combinations. The array elements that contain the highest number of votes indicate the presence of the shape. A circumference pattern is described by the parametric equation of the circumference, defined as

$$(x-a)^2 + (y-b)^2 = r^2 \tag{7}$$

where (a,b) are the coordinates of the circle center and r is the radius. So, the circular shapes present in I_{BM} can be obtained by performing the Circular Hough Transform on this image. It can be defined as

$$(P_c, r) = \mathrm{CHT}(I_{\mathrm{BM}}, r_{\min}, r_{\max}) \tag{8}$$

where $P_c = (i_c, j_c)$ and r are respectively the center position and the radius that define the circular shape with the highest punctuation in the Circular Hough Transform implemented by CHT. The radius r is restricted to be between $r_{\min}$ and $r_{\max}$, values which are one-tenth and one-fifth of the image [7] divided by two (as these measurements refer to OD diameter estimation). The minimum radius restriction reduces the probability of considering the OD cup, while the maximum radius restriction eliminates candidates with too wide areas. The obtained r value must be corrected due to the effects of (3) and (6). The vessel elimination performed in (3) enlarged the OD 27 pixels and the erosion operation in (6) produced a two-pixel reduction, so the r value has to be reduced by 25.

As previously commented, this processing is applied in parallel to the green and red channels. Thus, two OD approximations are obtained. The one with the higher score in the Circular Hough Transform algorithm is then selected as the definitive circular OD boundary approximation (Fig. 3, images R-5

TABLE I
RESULTS OF THE CIRCULAR HOUGH IN TERMS OF PERCENTAGE OF IMAGES PER OVERLAPPING INTERVAL AND AVERAGE OVERLAPPING OF THE WHOLE SET

	$S \geq 0.95$	$S \geq 0.90$	$S \geq 0.85$	$S \geq 0.80$	$S \geq 0.75$	$S \geq 0.70$	$\overline{S}$
"CircularGoldStandard"	27%	87%	96%	99%	99%	100%	0.92
CircularHough (this work)	**7%**	**46%**	**73%**	**84%**	**90%**	**93%**	**0.86**
Hausdorff-BasedTemplateMatching [21]*	2%	25%	45%	70%	77%	85%	0.81
CircularHough / "CircularGoldStandard"	**26%**	**53%**	**76%**	**85%**	**91%**	**93%**	**0.93**

* This results were obtained on a local database composed by 40 images.

and G-5). This score quantifies the point by point matching degree between the estimated circumference and the fitted shape in I_{BM}. Therefore, higher scores generally involve better OD border extraction and, hence, better segmentation quality. Moreover, the selection of the correct candidate is also favored by the fact that the score of this algorithm is an absolute and not a relative measure. This implies that the selected maximum-score criterion tends to select longer candidate circumferences. This is especially useful when the OD cup is wide enough to be considered a candidate, as it leads to an increased probability of selecting the correct candidate between the cup and the true OD boundary.

IV. TESTING AND RESULTS

We used in this study the publicly available MESSIDOR database [32], kindly provided by the Messidor program partners. It contains 1200 eye fundus color images of the posterior pole acquired by the Hôpital Lariboisière Paris, the Faculté de Médecine St. Etienne and the LaTIM–CHU de Brest (France). 800 of these images were captured with pupil dilation (one drop of Tropicamide at 10%) and 400 without dilation, using a Topcon TRC NW6 non-mydriatic retinograph with a 45° FOV. The images are 1440×960, 2240×1488, or 2304×1536 pixels in size and 8 bits per color plane and are provided in TIFF format. 540 images are from patients not affected by DR and 660 correspond to patients affected by the illness. To prevent the inclusion of any kind of skew, although some images are not suitable for processing (i.e., images too blurred or with severe enough cataract), no exclusion criteria was applied. To make evaluation of the algorithm performance on this database possible, the OD rim was manually delimited by experts producing by this way a gold standard set.

Although database images are provided in TIFF format, they were JPEG compressed at a ratio of 1:35 for testing. It was done for assessing algorithm performance under conditions established in the protocols defined by the organism that funded these investigations, the Andalusian Health Service, relating to image file size. This restriction is imposed as, using this kind of compressed format, storage requirements as well as latency in exchanging images via the internet are drastically reduced. Moreover, we performed tests on image resolution for the location and the segmentation methodologies, scaling down the images. These tests revealed that the results provided by both methods are independent and stable in spite of decreasing image resolution down to 300×300 for OD location and 640×640 for OD segmentation. Therefore, the methodologies presented are actually applied to images of these sizes. Any image of any resolution is reduced to 300×300 and 640×640 for OD location and OD segmentation respectively and the processes are performed scaling the window sizes and parameters to these resolutions. So, the results in this section were obtained applying these reductions.

Algorithm performance was evaluated by measuring the overlapping degree between the true OD regions in "gold standard" images and the approximated regions obtained with the described approach. The proposal by Lalonde *et al.* [21] was used with this purpose: an overlapping score S is defined to measure the common area between a true OD region T and a detected region D as

$$S = \frac{\mathrm{Area}\,(T \cap D)}{\mathrm{Area}\,(T \cup D)}. \tag{9}$$

Since the proposed algorithm segments the OD by approximating its shape by a circumference, for a better evaluation of its behavior, it is also interesting to get to know how far its results are from the maximum results reachable with this template-based approach. With this purpose, a "circular gold standard" set was created by calculating the best circular approximations for all true OD contours in the "gold standard" set by using (8). Then, the common area between the regions in the "gold standard" and these best circular approximations in the "circular gold standard" were calculated also according to (9). Therefore, the average of these values may be considered the upper limit of average common overlapping for an automatic OD segmentation using a circular approximation. So, generalizing, this experiment, apart from being interesting for better algorithm evaluation, provides an interesting objective measurement of the maximum OD area which can be covered by a circle. Therefore, it is an appropriate measure to assess the general suitability of OD segmentation using a circular approximation.

The algorithm presented in this paper (*CircularHough*) was applied to calculate the overlapping S defined in (9) for the 1200 images in the MESSIDOR database. This metric was also computed using the "circular gold standard" set (*CircularGoldStandard*). The results for both methods are summarized in Table I[1]. This table shows the percentage of images for different intervals of S values, as well as average overlapping $\overline{S}$ for the whole set of images. These overlapping measures corresponding to the *CircularHough* algorithm normalized by the results of the *CircularGoldStandard* are also shown in the last row. As shown in this table, overlapping between the hand-labelled OD region and *CircularHough* algorithm-segmented one is higher than or equal to 0.75% for 90% of the images in the database. Average

[1]Results of the experiment for every image is available at [33], in the Optic Disc Results subsection of the Results section

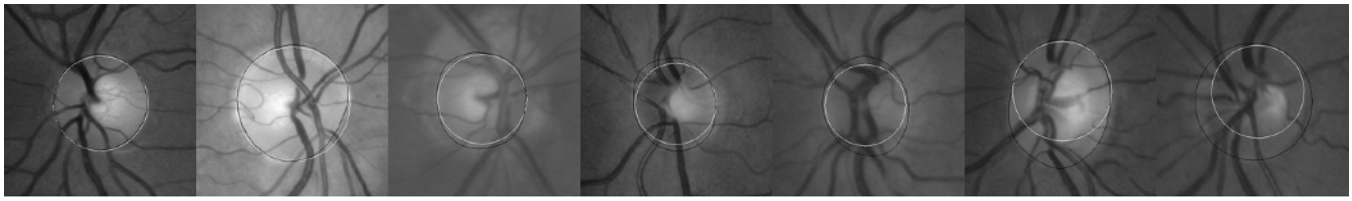

Fig. 4. Sample segmentations obtained with the presented methodology. (a) $S = 0.96$. (b) $S = 0.93$. (c) $S = 0.89$. (d) $S = 0.83$. (e) $S = 0.76$. (f) $S = 0.74$. (g) $S = 0.65$. White line: segmentations produced by the algorithm; black line: true OD areas labeled by specialists.

overlapping obtained for the whole set of images was 0.86. In this respect, note that the maximum overlapping reachable with a circular template-based approach is 0.92.

Fig. 4 shows segmentation examples obtained by the proposed methodology for all the overlapping intervals defined in Table I. It should be pointed out that, for segmentation algorithm testing, the location methodology presented in this paper was used to obtain the required initial OD location. This algorithm correctly found the OD in 1186 out of the 1200 images (99% success rate). OD location was manually determined in the 14 images in which the OD location algorithm failed.

The third row in Table I shows the performance results published by Lalonde *et al.* [21] for their circular template-based methodology. These results were obtained on a different database comprising 40 images taken from 27 patients attending a diabetic retinal-screening programme. As in the case of the MESSIDOR database, this set of images includes good, fair and bad visual quality images (Lalonde *et al.* considered bad quality images as those blurred and/or containing abnormally dark or bright regions). Our algorithm could not be tested on this database as we had no access to it. The algorithm proposed by Lalonde *et al.* (*Hausdorff-BasedTemplateMatching*) is based on minimizing the Hausdorff distance between previously obtained candidate edge map regions and a set of circular templates. As it can be observed, the *CircularHough* method exceeds the results of this methodology for all considered overlapping intervals and also enhances average overlapping.

Finally, tests concerning computational efficiency were also done. The tests were performed on a current midrange PC equipped with an Intel Core2Duo CPU at 2.13 GHz and 2 GB of RAM capacity. The algorithms were implemented in Java programming language and tested running on the Java Virtual Machine version 6. For a total of 1200 executions of the algorithm for OD segmentation, the average computational time obtained was 5.69 s. with a standard deviation of 0.54 s. The average computational time obtained for OD location was 1.67 s. with a standard deviation of 0.14 s.

V. Discussion on OD Segmentation Models

In this section, we discuss on the advantages and disadvantages of the most widely-used OD segmentation models: circular as well as elliptical template-based methods and deformable model-based methods. The first discussion focuses on the use of elliptical or circular models. For that, four different elliptical approaches were implemented and tested to compare them to the circular approximation presented here. In the second subsection, the proposed circular approach is compared to three deformable model-based algorithms and obtained results are discussed.

TABLE II
Comparison of Segmentation Potential of Different Models in Terms of Average Overlapping

	$\overline{S}$
Deformable Models	100%
Elliptical Template-Based Models	97%
Circular Template-Based Models	92%

A. The Presented Circular Template-Based Method Versus The Elliptical Template-Based Approach

According to OD shape features, the use of an elliptical model for OD segmentation, at least theoretically, should render higher segmentation potential. For empirical evaluation of this issue, the experiment used for circular model potential assessment was now reproduced and applied to elliptical models. That is, an "elliptical gold standard" set was generated by applying an elliptical model for fitting the true OD contours in the "gold standard" set of the database described in Section IV. So, the average overlapping of both sets may be considered the maximum segmentation potential of an elliptical model. Table II summarizes the potential of all models discussed in this section. As it can be observed, the use of an elliptical model renders a theoretical overlapping increase of 5% relative to the potential rendered by a circular model. Nevertheless, since the elliptical approach has two degrees-of-freedom more than the circular model (rotation angle and additional radius), its results may show a less robust and stable behavior.

To assess elliptical model behaviour, four elliptical template-based variants were implemented and applied to the I_{BM} obtained from operation (6). Three of these approaches were based on minimizing the algebraic distance [34], [35] and one was based on minimizing the geometric distance [34]. Each approach was tested on the database used in Section IV and results were measured using the metric defined in (9). Thus, the elliptical and circular approaches can be compared under the same conditions. Table III summarizes the results obtained in this test. Data are presented in columns as the percentage of images per interval of overlapping values, the penultimate column is the total average overlapping and the last one indicates the percentage of model-solved cases, as the tested methods do not always converge to a solution. The first row shows the results for the elliptical approach based on minimizing the geometric distance, the following three rows show the results obtained

TABLE III
COMPARISON BETWEEN THE PRESENTED CIRCULAR TEMPLATE-BASED METHOD AND FOUR ELLIPTICAL TEMPLATE-BASED APPROACHES. DATA IN TERMS OF PERCENTAGE OF IMAGES PER OVERLAPPING INTERVAL AND AVERAGE OVERLAPPING OF THE WHOLE SET

	$S \geq 0.95$	$S \geq 0.90$	$S \geq 0.85$	$S \geq 0.80$	$S \geq 0.75$	$S \geq 0.70$	$\overline{S}$	SF^*
EllipticalGeometricalMin [34]	2%	11%	20%	30%	39%	51%	0.67	89%
EllipticalAlgebraicMin1 [35]	2%	9%	17%	26%	36%	48%	0.66	99%
EllipticalAlgebraicMin2 [34]	2%	10%	19%	27%	36%	47%	0.65	87%
EllipticalAlgebraicMin3 [34]	2%	9%	18%	26%	35%	48%	0.66	98%
CircularHough (this work)	**7%**	**46%**	**73%**	**84%**	**90%**	**93%**	**0.86**	100%

* SF (Solutions Found): percentage of cases for which the model found a solution.

with the three variants based on minimizing the algebraic distance, and the last row show the results of the circular approach presented in this paper. Importantly, the average values for each elliptical method were calculated considering only the cases for which they had found a solution. Another important issue with regard to results is that no automated criterion was used for selecting for each image between the segmentations from the red and green channels. For each image, both candidates were measured and the one with the highest overlapping score was selected for method total average calculation. Hence, the results shown in Table III are the highest possible scores for each elliptical approach.

The results from this study indicate that the segmentation performance of all elliptical approaches is similar. The greater difference between them was observed at the percentage of solved cases. Interestingly, their performance is significantly poorer than that obtained with the circular model. This performance degradation is the result of elliptical models's higher sensitivity to poor OD border contrast and, therefore, to poor border extraction. These models require the extraction of a great amount of OD representative borders to provide correct estimations of the two radiuses and rotation angle. On the other hand, the circular model proposed in this paper only needs some portions of the OD contour to obtain a fitting circumference. Although the preprocessing designed in this work may not be the most appropriate for elliptical models, their direct application for OD segmentation is suggested here to offer less stable and homogeneous behavior.

B. The Presented Circular Template-Based Method Versus the Deformable Model-Based Approach

The main advantage of using a deformable model instead of a template-based model for OD segmentation is that, theoretically, 100% of overlapping areas between the automated segmentation and the ground truth may be achieved. As shown in Table II, it involves an 8% increase relative to a circular model. This is why deformable models have much more degrees-of-freedom than template-based models to fit the desired shape. However, these additional freedom degrees-of-freedom make these models more sensitive to irregular or low OD boundary contrast.

As a basis for this discussion, the template-based method proposed here was compared to the three OD segmentation approaches based on deformable models proposed by Lowell *et al.* in [18]. For the sake of comparison rigorousness, we used the same database, "gold standard" set and metric as those used in this work. Thus, the algorithms can be compared under identical

TABLE IV
COMPARISON BETWEEN THE PRESENTED CIRCULAR TEMPLATE-BASED METHOD AND THREE DEFORMABLE MODEL-BASED APPROACHES IN TERMS OF PERCENTAGE OF IMAGES PER SUBJECTIVE CATEGORY

	Excellent	Good	Fair	Poor	Excellent-Fair
CircularHough	**40%**	**39%**	**18%**	**3%**	**97%**
TemporalLock [18]	42%	31%	10%	17%	83%
DV-Hough [18]	39%	22%	20%	19%	81%
Simple [18]	9%	8%	30%	53%	47%

conditions. The database is composed of 90 images acquired at a resolution of 640×480 and 8 bits per color plane. These images were taken from 50 patients, 19 of them being affected by type 2 diabetes mellitus; the diabetes status was unavailable for the remaining 31. To produce the "gold standard" segmentation for this set of images, four clinicians manually delimited the rim for each image, and the mean and radial standard deviations of these contours were calculated. Then, Lowell *et al.* defined the discrepancy δ^j as

$$\delta^j = \sum_i \frac{m_i^j - \mu_i^j}{\sigma_i^j - \epsilon} \tag{10}$$

where μ_i^j and σ_i^j summarize the clinicians choice of rim location on spoke i of image j and m_i^j is segmentation location on spoke i for image j. Spokes are points belonging to the OD rim; 24 spokes were considered taken each 15°. Division by σ compensates for uncertainty in rim position and ϵ is a small factor to prevent division by zero where the clinicians are in exact agreement. In addition to this measure, they defined four categories corresponding to their subjective perception of quality. These four categories are *Excellent*, *Good*, *Fair*, and *Poor*, referencing images with disparity up to one, two, five, or more, respectively. They assessed their algorithms performance considering the percentage of segmentations classified in the range *Excellent–Fair*.

Table IV summarizes the performance on this subjective scale for their three alternative algorithms and the one proposed in this paper. Results are expressed in terms of the percentage of images per subjective category. As it can be observed, with the best deformable model approach, 2% more of excellent segmentations were obtained than with the presented approach. Nevertheless, the template-based approach provided a significant enhancement in the percentage of obtained "valid" segmentations, thus reaching the 79% versus 73% of segmentations within the *Excellent–Good* range, and 97% versus 83% of segmentations within the *Excellent–Fair* range.

The results of this experiment, in spite of not being applicable to all template-based and deformable models, are a good example of comparable segmentation performance of both approaches on a particular common case. Therefore, the main conclusion of this experiment would be that, for OD segmentation, under appropriate OD background-contrast conditions, deformable models render more accurate OD segmentations. On the contrary case, when contrast conditions are not so favourable, the circular approach may turn out to be a more robust and reliable solution.

VI. Discussion and Conclusion

This paper presents a new template-based approach for OD segmentation by means of a circular OD-boundary approximation. In addition, an OD location methodology for obtaining the OD position needed by the segmentation algorithm as initial information is also proposed.

The results presented in this paper show that the proposed methodology offers a reliable and robust solution for OD segmentation. According to the results in Table I, the overlapping between the "true" OD region and the one segmented by our algorithm is over 0.75 in 90% of the 1200 MESSIDOR images, being the average overlapping 0.86 for the whole set of images. This result is more valuable taking into account that maximum overlapping with a circular template-based approach is 0.92. Referentially, it can be pointed out that performance comparisons with the circular template-based approach by Lalonde *et al.* [21] show that the overlapping obtained by our proposal was clearly higher, in spite of the fact that our results were obtained on a set of 1200 images while Lalonde *et al.* used only 40 (results are shown in Table I).

Moreover, discussion in Section V on different OD segmentation, strengthens the hypothesis of the suitability of circular models for this purpose. The tests summarized in Table II indicate that the overlapping area between ground-truth OD segmentations and those obtained by elliptical models is higher than those obtained by circular models (97% and 92%, respectively). However, when testing with numerous and different real cases, the simplicity of the presented circular model generally favours obtaining a more robust behaviour. Thus, performance comparisons between the proposed circular template-based method and four elliptical template-based approaches for the MESSIDOR images (Table III) indicate that the circular approach renders a clearly higher average overlapping. The same conclusion was drawn for deformable models. Although these models can theoretically obtain 100% overlapping, the performance results presented in terms of discrepancy grades in Table IV, indicate that our proposed circular model outperforms the deformable model proposed by Lowell *et al.* in [18].

On the other hand, it must be mentioned that, to facilitate performance comparison between OD segmentation methods, the generated hand segmentations of the OD rim for the 1200 images in the MESSIDOR database are currently available for researchers at [33], in the Sample Databases subsection within the Results section by selecting the MESSIDOR database. The original database is available at [32]. To the best of our knowledge, such a set of "gold standard" images from a clinically labelled database is not available for the research community at the present time.

The main conclusions of this work can be summarized as follows.

1) The performance results obtained by the proposed methodology on a huge digital retinal database indicate that simple methods, based on basic image processing techniques, seem to suffice for OD location and segmentation.
2) A circular modelling for the OD boundary, compared to elliptical and deformable models, was shown to offer good compromise between success rate, quality and efficiency, as shown by comparing its segmented area to experts' free-drawn areas.

Despite all of this, the existence of some specific cases in which, due to their exceptional ellipsity degree, the circular approach does not reach the performance results of the elliptical approach has been reported [see, for instance, the case in Fig. 4(f)]. With the aim of enhancing the overlapping rates obtained in this work for these isolated cases, the authors' current research is focused on the development of a methodology for performing a controlled elliptical deformation of the obtained circumference. Within the framework of this study, whether any preprocessing modification is necessary or even whether postprocessing would be appropriate for assuring deformation process stability is currently under study.

Acknowledgment

The authors would like to thank the Messidor program partners for facilitating their database. Special thanks to Dr. A. Hunter for his generosity, as he provided us with the material which made possible the study presented in Section V-A.

References

[1] H. R. Taylor and J. E. Keeffe, "World blindness: A 21st century perspective," *Br. J. Ophthalmol.*, vol. 85, pp. 261–266, 2001.
[2] S. Wild, G. Roglic, A. Green, R. Sicree, and H. King, "Global prevalence of diabetes: Estimates for the year 2000 and projections for 2030," *Diabetes Care*, vol. 27, pp. 1047–1053, 2004.
[3] D. Klonoff and D. Schwartz, "An economic analysis of interventions for diabetes," *Diabetes Care*, vol. 23, pp. 390–404, 2000.
[4] N. Patton, T. M. Aslam, T. MacGillivray, I. J. Deary, B. Dhillon, R. H. Eikelboom, K. Yogesan, and I. J. Constable, "Retinal image analysis: Concepts, applications and potential," *Prog. Retin. Eye Res.*, vol. 25, pp. 99–127, 2006.
[5] A. Singalavanija, J. Supokavej, P. Bamroongsuk, C. Sinthanayothin, S. Phoojaruenchanachai, and V. Kongbunkiat, "Feasibility study on computer-aided screening for diabetic retinopathy," *Jpn. J. Ophthalmol.*, vol. 50, pp. 361–366, 2006.
[6] C. Sinthanayothin, J. F. Boyce, H. L. Cook, and T. H. Williamson, "Automated localisation of the optic disc, fovea, and retinal blood vessels from digital colour fundus images," *Br. J. Ophthalmol.*, vol. 83, pp. 902–910, 1999.
[7] H. Li and O. Chutatape, "Automatic location of optic disc in retinal images," in *Proc. IEEE Int. Conf. Image Process.*, 2001, pp. 837–840.
[8] L. Gagnon, M. Lalonde, M. Beaulieu, and M. C. Boucher, "Procedure to detect anatomical structures in optical fundus images," in *Proc. Conf. Med. Imag. 2001: Image Process.*, San Diego, CA, 2001, pp. 1218–1225.
[9] A. Osareh, M. Mirmehdi, B. Thomas, and R. Markham, "Automated identification of diabetic retinal exudates in digital colour images," *Br. J. Ophthalmol.*, vol. 87, pp. 1220–1223, 2003.
[10] H. A. Quigley and A. T. Broman, "The number of people with glaucoma worldwide in 2010 and 2020," *Br. J. Ophthalmol.*, vol. 90, pp. 262–267, 2006.

[11] H. Li and O. Chutatape, "A model-based approach for automated feature extraction in fundus images," in *Proc. 9th IEEE Int. Conf. Comput. Vis. (ICCV'03)*, 2003, vol. 1, pp. 394–399.

[12] C. Sinthanayothin, "Image analysis for automatic diagnosis of diabetic retinopathy," Ph.D. dissertation, Univ. London, London, U.K., 1999.

[13] A. Hoover and M. Goldbaum, "Locating the optic nerve in a retinal image using the fuzzy convergence of the blood vessels," *IEEE Trans. Med. Imag.*, vol. 22, no. 8, pp. 951–958, Aug. 2003.

[14] A. Hoover and M. Goldbaum, "Fuzzy convergence," in *Proc. IEEE Comput. Soc. Conf. Comput. Vis. Pattern Recognit.*, Santa Barbara, CA, 1998, pp. 716–721.

[15] M. Foracchia, E. Grisan, and A. Ruggeri, "Detection of optic disc in retinal images by means of a geometrical model of vessel structure," *IEEE Trans. Med. Imag.*, vol. 23, no. 10, pp. 1189–1195, Oct. 2004.

[16] A. A. H. A. R. Youssif, A. Z. Ghalwash, and A. R. Ghoneim, "Optic disc detection from normalized digital fundus images by means of a vessels' direction matched filter," *IEEE Trans. Med. Imag.*, vol. 27, pp. 11–18, 2008.

[17] A. Osareh, M. Mirmehdi, B. Thomas, and R. Markham, "Comparison of colour spaces for optic disc localisation in retinal images," in *Proc. 16th Int. Conf. Pattern Recognit.*, 2002, pp. 743–746.

[18] J. Lowell, A. Hunter, D. Steel, A. Basu, R. Ryder, E. Fletcher, and L. Kennedy, "Optic nerve head segmentation," *IEEE Trans. Med. Imag.*, vol. 23, no. 2, pp. 256–264, Feb. 2004.

[19] J. Xu, O. Chutatape, E. Sung, C. Zheng, and P. C. T. Kuan, "Optic disk feature extraction via modified deformable model technique for glaucoma analysis," *Pattern Recognit.*, vol. 40, no. 7, pp. 2063–2076, 2007.

[20] D. W. K. Wong, J. Liu, J. H. Lim, X. Jia, F. Yin, H. Li, and T. Y. Wong, "Level-set based automatic cup-to-disc ratio determination using retinal fundus images in ARGALI," in *Proc. 30th Annu. Int. IEEE EMBS Conf.*, 2008, pp. 2266–2269.

[21] M. Lalonde, M. Beaulieu, and L. Gagnon, "Fast and robust optic disk detection using pyramidal decomposition and Hausdorff-based template matching," *IEEE Trans. Med. Imag.*, vol. 20, no. 11, pp. 1193–1200, Nov. 2001.

[22] T. Walter and J. C. Klein, "Segmentation of color fundus images of the human retina: Detection of the optic disc and the vascular tree using morphological techniques," in *Proc. 2nd Int. Symp. Med. Data Anal.*, 2001, pp. 282–287.

[23] A. W. Reza, C. Eswaran, and S. Hati, "Automatic tracing of optic disc and exudates from color fundus images using fixed and variable thresholds," *J. Med. Syst.*, vol. 33, pp. 73–80, 2008.

[24] M. D. Abràmoff, W. L. M. Alward, E. C. Greenlee, L. Shuba, C. Y. Kim, J. H. Fingert, and Y. H. Kwon, "Automated segmentation of the optic disc from stereo color photographs using physiologically plausible features," *Invest. Ophthalmol. Vis. Sci.*, vol. 48, no. 4, pp. 1665–1673, 2007.

[25] T. Walter and J. C. Klein, "Automatic analysis of color fundus photographs and its application to the diagnosis of diabetic retinopathy," in *Handbook of Biomedical Image Analysis*. New York: Kluwer, 2005, vol. 2, pp. 315–368.

[26] N. Otsu, "A threshold selection method from gray-scale histogram," *IEEE Trans. Syst. Man Cybern.*, vol. 8, pp. 62–66, 1978.

[27] C. Heneghan, J. Flynn, M. O'Keefe, and M. Cahill, "Characterization of changes in blood vessel width and tortuosity in retinopathy of prematurity using image analysis," *Med. Image Anal.*, vol. 6, pp. 407–429, 2002.

[28] R. C. Gonzalez and R. E. Woods, "Image Segmentation," in *Digital Image Processing*, 2nd ed. Upper Saddle River, NJ: Prentice-Hall, 2002, pp. 577–581.

[29] P. V. C. Hough, "Methods and means for recognizing complex patterns," U.S. Patent 3 069 654, Dec. 1962.

[30] R. O. Duda and P. E. Hart, "Use of the Hough transformation to detect lines and curves in picture," *Commun. ACM*, vol. 15, pp. 11–15, 1972.

[31] C. Kimme, D. Ballard, and J. Sklansky, "Finding circles by an array of accumulators," *Commun. Assoc. Comput. Mach.*, vol. 18, pp. 120–122, 1975.

[32] *Download Images Section, MESSIDOR: Digital Retinal Images, MESSIDOR TECHNO-VISION Project, France*, [Online]. Available: http://messidor.crihan.fr/download-en.php

[33] Expert system for early automated detection of DR by analysis of digital retinal images project website. Huelva, Spain, Univ. Huelva [Online]. Available: http://www.uhu.es/retinopathy

[34] W. Gander, G. H. Golub, and R. Strebel, "Least square fitting of circles and ellipses," *BIT*, no. 43, pp. 558–578, 1994.

[35] A. Fitzgibbon, M. Pilu, and R. B. Fisher, "Direct least square fitting of ellipses," *IEEE Trans. Pattern Anal. Mach. Intell.*, vol. 21, no. 5, pp. 476–480, May 1999.